

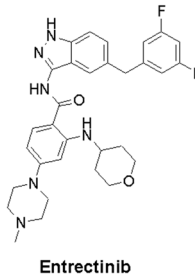
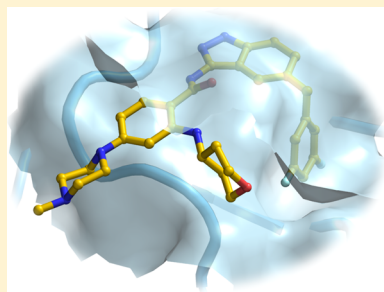
Discovery of Entrectinib: A New 3-Aminoindazole As a Potent Anaplastic Lymphoma Kinase (ALK), c-ros Oncogene 1 Kinase (ROS1), and Pan-Tropomyosin Receptor Kinases (Pan-TRKs) inhibitor

Maria Menichincheri,^{*,†} Elena Ardin,[†] Paola Magnaghi,[†] Nilla Avanzi,[†] Patrizia Banfi,[†] Roberto Bossi,^{†,§} Laura Buffa,[†] Giulia Canevari,[†] Lucio Ceriani,[†] Maristella Colombo,[†] Luca Corti,[†] Daniele Donati,[†] Marina Fasolini,[†] Eduard Felder,[†] Claudio Fiorelli,^{†,||} Francesco Fiorentini,[†] Arturo Galvani,[†] Antonella Isacchi,[†] Andrea Lombardi Borgia,[†] Chiara Marchionni,[†] Marcella Nesi,[†] Christian Orrenius,[†] Achille Panzeri,[†] Enrico Pesenti,[‡] Luisa Rusconi,[†] Maria Beatrice Saccardo,[†] Ermes Vanotti,[†] Ettore Perrone,[†] and Paolo Orsini[†]

[†]Oncology, Nerviano Medical Sciences Srl, Viale Pasteur 10, 20014 Nerviano, Milan, Italy

[‡]Accelera Srl, Viale Pasteur 10, 20014 Nerviano, Milan, Italy

Supporting Information



Biochemical data

ALK IC ₅₀	= 0.012 μM
ROS-1 IC ₅₀	= 0.007 μM
TRKA IC ₅₀	= 0.001 μM
TRKB IC ₅₀	= 0.003 μM
TRKC IC ₅₀	= 0.005 μM

ABSTRACT: Anaplastic lymphoma kinase (ALK) is a receptor tyrosine kinase responsible for the development of different tumor types. Despite the remarkable clinical activity of crizotinib (Xalkori), the first ALK inhibitor approved in 2011, the emergence of resistance mutations and of brain metastases frequently causes relapse in patients. Within our ALK drug discovery program, we identified compound 1, a novel 3-aminoindazole active on ALK in biochemical and in cellular assays. Its optimization led to compound 2 (entrectinib), a potent orally available ALK inhibitor active on ALK-dependent cell lines, efficiently penetrant the blood–brain barrier (BBB) in different animal species and highly efficacious in *in vivo* xenograft models. Moreover, entrectinib resulted to be strictly potent on the closely related tyrosine kinases ROS1 and TRKs recently found constitutively activated in several tumor types. Entrectinib is currently undergoing phase I/II clinical trial for the treatment of patients affected by ALK-, ROS1-, and TRK-positive tumors.

INTRODUCTION

Oncogenic forms of protein kinases have been described in different human tumor types and acting as drivers in specific genetic contexts define subsets of patients that are highly responsive to kinase inhibitors such as imatinib in BCR-ABL positive chronic myelogenous leukemia (CML) and erlotinib in epidermal growth factor receptor (EGFR)-mutated nonsmall cell lung cancer (NSCLC).^{1,2} The anaplastic lymphoma kinase (ALK), a receptor tyrosine kinase (RTK) belonging to the insulin receptor superfamily, is a well validated target based on preclinical and clinical studies.^{3,4}

A constitutively activated, oncogenic form of ALK has been first found in a subset of anaplastic large cell lymphoma (ALCL), namely the chimeric protein NPM-ALK, resulting from a chromosomal translocation, which causes the fusion of the N-terminal portion of the normally expressed protein nucleophosmin (NPM) to the ALK kinase domain.⁵ Sub-

sequently, additional ectopically expressed, activated fusion forms of ALK have been identified and recognized as potent oncogenic drivers in other tumor types such as inflammatory myofibroblastic tumors (IMT)⁶ and, most importantly, in a subset of NSCLC patients where they account for nearly 3–7% of cases.^{7,8} The majority of ALK-positive NSCLC harbors the same intrachromosomal rearrangement that results in the expression of EML4–ALK chimeric protein, generated from the fusion of the N-terminal portion of echinoderm microtubule-associated protein-like-4 (EML4) and the ALK kinase domain. ALK fusion partners invariably provide a protein/protein interaction domain that induces ALK oligomerization and leads to constitutive activation of the tyrosine kinase.⁷ Other tumorigenic forms of the ALK kinase are due to the

Received: January 14, 2016

Published: March 22, 2016

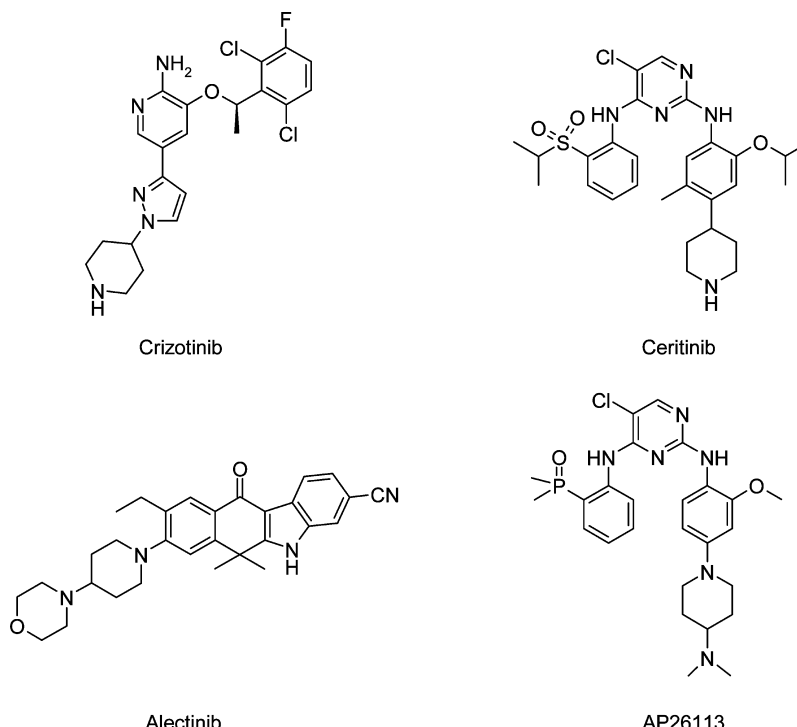


Figure 1. Structures of the most advanced ALK inhibitors.

acquisition of single point mutations that lead to the expression of activated forms of the full-length receptor, as reported for example in both familial and sporadic neuroblastoma.⁹⁻¹²

With ALK being a well validated target in oncology for many years, several ALK inhibitors have been identified and entered clinical trials such as crizotinib from Pfizer,¹³ ceritinib from Novartis,¹⁴ alectinib from Chugai/Roche,¹⁵ and AP26113 from Ariad¹⁶ (Figure 1). All these compounds demonstrated striking clinical efficacy in ALK-positive selected patient population already during the initial phases of clinical development, and the most advanced ones have reached the registration for ALK-dependent cancers. First, crizotinib has been approved in 2011 for the treatment of ALK-positive NSCLC patients, followed by ceritinib and alectinib. Ceritinib has been approved in 2014 for the treatment of ALK-positive, metastatic NSCLC patients relapsed from or intolerant to crizotinib and alectinib has been granted accelerated approval in 2015 by the Food and Drug Administration (FDA) for the treatment of ALK-positive NSCLC patients who progressed after crizotinib treatment.

However, despite the initial clinical benefit demonstrated in specific clinical settings with ALK inhibitors, relapse was invariably observed in all treated patients. On the basis of clinical experience accumulated to date with crizotinib, it clearly emerged that low brain penetration represents a major weakness of this drug and appearance of brain metastases is a demonstrated cause of disease recurrence in crizotinib-treated patients.¹⁷ In addition, the emergence of mutations in the ALK kinase domain that confer resistance to the drug was reported for the first as well as the second generation ALK inhibitors.¹⁸⁻²⁰

Because of the relevant role of the ALK oncogene in different tumor settings, we performed a high-throughput screening (HTS) of our Corporate Compound Collection with the aim to identify suitable hits for further optimization as ALK kinase inhibitors. Among different hits, the 3-amino-5-substituted indazole **1** emerged as a promising starting point for further

investigation (Figure 2). This compound showed a good biochemical potency against the ALK kinase ($IC_{50} = 0.073 \mu M$)

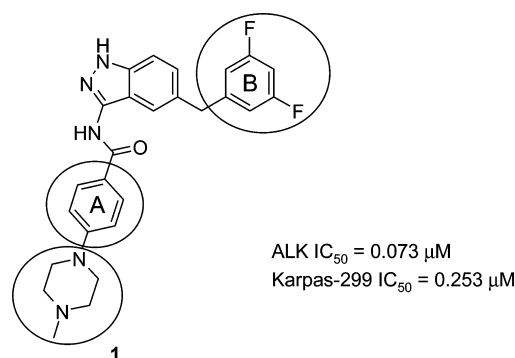


Figure 2. Structure of the starting hit compound 1.

and an appreciable antiproliferative activity on the ALK-dependent ALCL Karpas-299 cell line ($IC_{50} = 0.253 \mu M$).

The chemical structure of **1** was considered amenable to structural modifications, which we believed to be potentially suitable for improvement of its biological activity. Among the available options, we focused our attention on the substitution pattern of the fluorinated phenyl ring B, the introduction of substituents on ring A, and the modification of the *N*-methylpiperazinyl solubilizing group at the *para* position of ring A.

Here we describe the optimization process of compound 1 toward our final candidate compound 2 (entrectinib, Figure 3), a potent ALK inhibitor characterized by good oral absorption in rodent and nonrodent animal species and good efficacy in *in vivo* animal tumor models. Most importantly, compound 2 turned out to be a highly potent inhibitor of the closely related RTKs ROS1 and TRKs that were recently found rearranged in different tumor types. The expression of oncogenic fusion

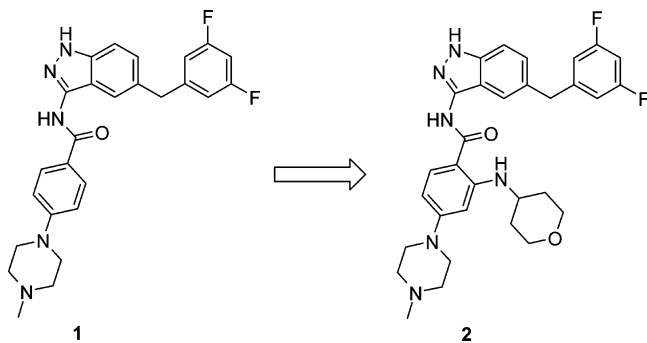


Figure 3. Modification of the starting hit **1** toward the final candidate **2**.

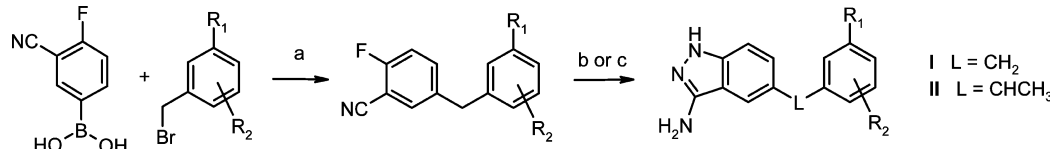
proteins containing constitutively activated ROS1 kinase domain have been identified in a subset of NSCLC patients (1–2% of cases).²¹ Analogously chromosomal rearrangements involving the neurotrophic tyrosine receptor kinase 1 gene (NTRK1), which encodes for the high affinity nerve growth factor (NGF) receptor tropomyosin receptor kinase A (TRKA), have been found in around 12% of papillary thyroid carcinoma²² and very recently reported in a subset of NSCLC²³ and colorectal carcinoma (CRC) patients²⁴ as well as in additional tumor types (Spitz tumors,²⁵ intrahepatic cholangiocarcinoma,²⁶ glioblastoma,²⁷ and pediatric high grade glioma²⁸). Although the frequency of such events in these neoplastic diseases remains to be defined due to the low number of patients screened so far, these findings support the rationale for targeted therapy with TRKA inhibitors in selected patient populations. Thus, the activity of compound **2** on these kinases represents a major opportunity for clinical development of the compound in additional ROS1- and TRK-dependent clinical settings. On the basis of these findings, together with the preclinical data in different models, compound **2** is currently undergoing phase I/II clinical trials for the treatment of patients affected by ALK-, ROS1-, and TRK-positive tumors where it has already shown remarkable activity.^{29,30}

■ CHEMISTRY

Target compounds were obtained by coupling either scaffold **I** or **II** (Scheme 1) with benzoic acid derivatives of general formula **III** (Scheme 2 and Scheme 3). Key step in the synthesis of intermediates **I** and **II** is the Suzuki–Miyaura cross-coupling reaction between different substituted benzyl bromides and commercially available 3-cyano-4-fluorophenylboronic acid in the presence of $Pd(PPh_3)_4$ complex as a catalyst and K_3PO_4 as a base.³¹

Methyl group in scaffold **II** has been introduced by reaction of the corresponding diarylmethane with methyl iodide and LiHMDS.

Scheme 1. Synthesis of 5-Benzyl-indazoles **I** and **II**^a



^aConditions: (a) $Pd(PPh_3)_4$, K_3PO_4 , toluene, 100 °C; (b) $NH_2NH_2 \cdot H_2O$, *n*-BuOH, 120 °C; (c) CH_3I , LiHMDS, THF then $NH_2NH_2 \cdot H_2O$, *n*-BuOH, 120 °C.

Synthesis of 3-acylamino-5-benzyl indazoles is outlined in Scheme 2 and Scheme 3. Activation of properly protected carboxylic acids **III** with oxalyl chloride, followed by reaction with intermediates **I** or **II** at low temperature, gave regioselective acylation at the 3-amino group of the scaffold.³²

Removal of the trifluoroacetamido protecting group provided the desired target molecules **2**, **3**, **5–10**, **12–16**, **18**, **20–25**, and **28–31**. Amino group in compound **4** was obtained by reduction of the corresponding nitro derivative **3**. Compound **11** required an additional deprotection step to remove the silyloxy protecting group by using TBAF in THF. Compounds **17** and **19** were obtained by hydrolysis of the benzoic group under standard basic conditions ($LiOH$, water, methanol). Enantiomers **26** and **27** were separated by preparative chiral HPLC from racemic derivative **25**, but the absolute configuration of the stereocenter has not been evaluated.

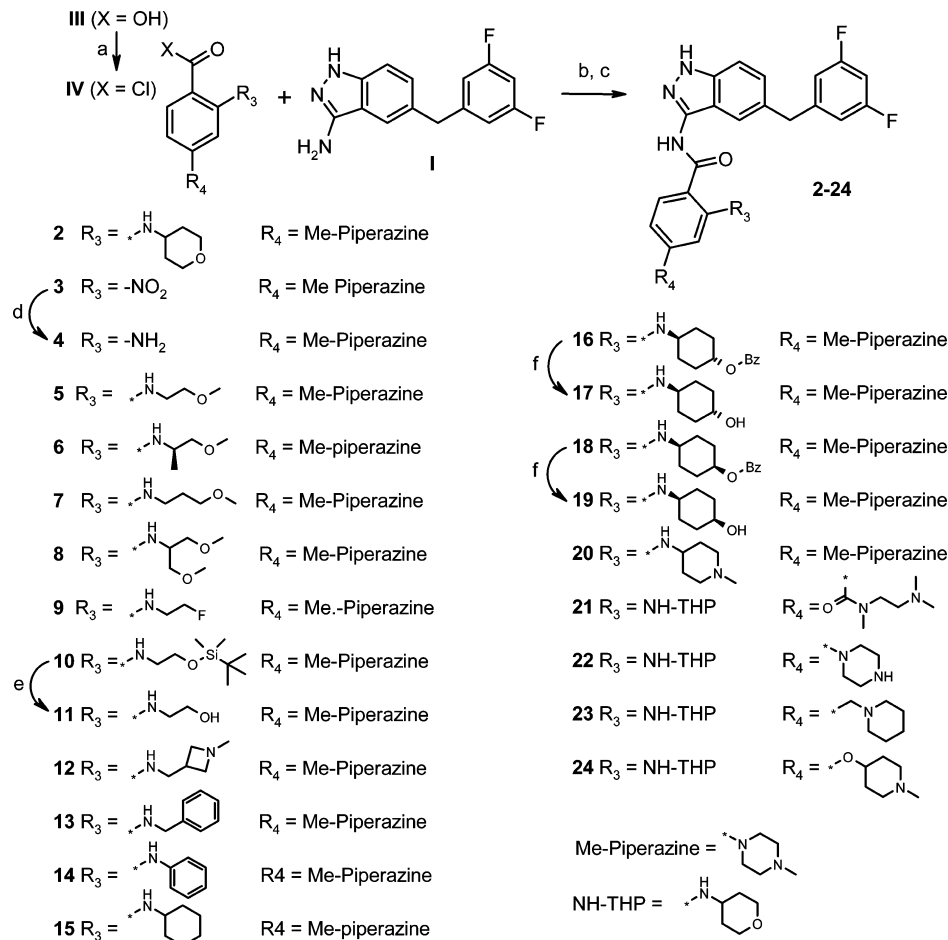
■ RESULTS AND DISCUSSION

Structure Based Design. To design new ALK inhibitors starting from compound **1**, we took advantage of the in-house available structure of the ALK kinase in complex with the weak prototype ALK inhibitor PHA-E429³³ (see Figure 4, right panel).

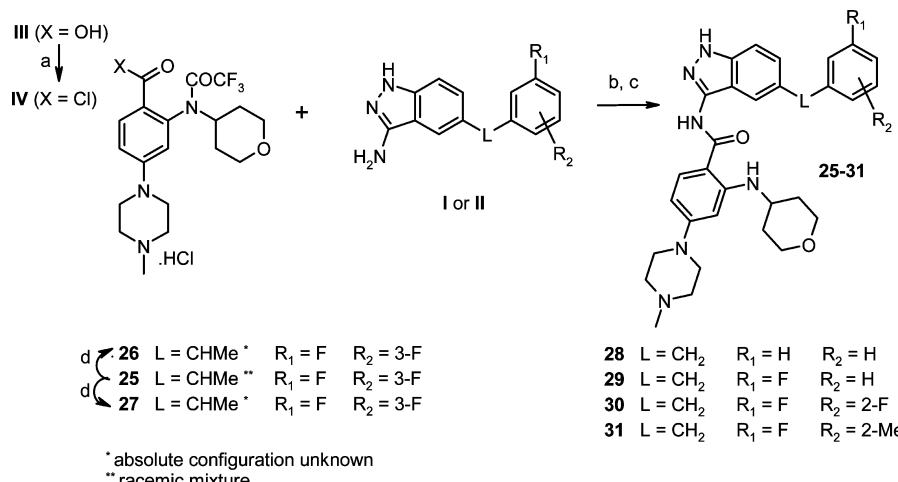
Analysis of this structure suggests that appropriately mono substituted A ring at position 2' (Figure 4, left panel) would yield derivatives occupying an area in and around the adenosine triphosphate (ATP) sugar pocket while displacing the observed water molecule W1 (Figure 4, right panel). In particular, NH-R substituents at that position of ring A were predicted to achieve this result while stabilizing the bioactive conformation through an intramolecular hydrogen bond involving the hydrogen of the *ortho* amino group and the carbonyl of the adjacent carboxamido group (Figure 4, left panel).

As far as the nature of the group R is concerned, a combined medicinal chemistry and docking strategy using sugar-resembling substituents led to the prioritization of saturated aliphatic rings containing nitrogen, oxygen, or hydroxyl groups. Such cyclic R substituents were expected to rotate with respect to the plane of the hinge binder optimally filling the available space, thus making contact interactions with both the catalytic loop “floor” and the Gly-rich loop “ceiling” of the ATP-binding site. Branched aliphatic chains were also considered but were expected to be less promising due to their flexibility. This approach produced a subset of new compounds driving both biochemical and cellular potencies in the desired direction (see Table 1 and further discussion). In particular, compound **2** emerged as one of the most interesting compounds in terms of biochemical potency, with the tetrahydropyranyl ring at position 2' of phenyl ring A displaying an optimal fitting within the ATP sugar pocket.

The 2.2 Å structure of ALK in complex with compound **2** (Figure 5) was indeed in agreement with the above

Scheme 2. Synthesis of Benzoyl-Modified 3-Acylamino-5-benzyl Indazoles 2–24^a

^aConditions: (a) $(COCl)_2$, DCM, DMF; (b) DIPEA, THF, $-20\text{ }^{\circ}\text{C}$; (c) MeOH, TEA; (d) cyclohexene. Pd/C, dioxane; (e) TBAF, THF; (f) LiOH· H_2O , MeOH, water.

Scheme 3. Synthesis of Benzyl-Modified 3-Acylamino-5-benzyl Indazoles 25–31^a

^aConditions: (a) $(COCl)_2$, DCM, DMF; (b) DIPEA, THF, $-20\text{ }^{\circ}\text{C}$; (c) MeOH, TEA; (d) chiral HPLC.

expectations based on the modeling prediction. The compound is anchored to the hinge region via the canonical donor–acceptor–donor hydrogen bonding motif between the nitrogens on the aminoindazole moiety and the backbone of residues Glu1197 and Met1199. The difluorobenzyl-indazole

core of the compound also makes favorable contacts with Leu1256, Leu1122, Val1130, and the gatekeeper Leu1196. The glycine-rich loop adopts a peculiar “collapsed” conformation, which was not previously reported in publicly available ALK structures, so that the 3,5-difluorobenzyl moiety is favorably

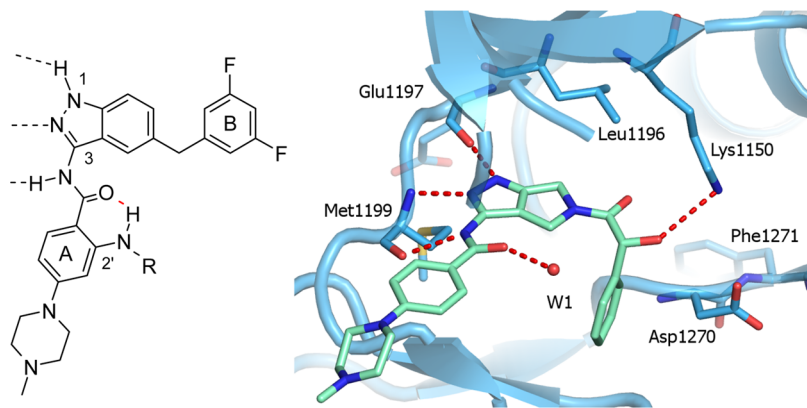


Figure 4. (left) Predicted H-bond interaction suitable to stabilize the bioactive conformation of this chemical template. (right) ATP-binding site occupied by PHA-E429 (PDB ID 2XBA) with the observed water molecule W1 (red sphere).

stacked between Leu1256 and Phe1127 from the glycine-rich loop. Moreover, the fluorine atom pointing toward the interior of the pocket is involved in multipolar interactions with the backbone carbonyls of Gly1269 (DFG-1 residue) and Asn1254. The phenyl ring A makes a hydrophobic contact with the glycine-rich loop residue Leu1122, while the methylpiperazine moiety protrudes into the solvent. As expected, the partially solvent-exposed tetrahydropyranyl moiety adopts a roughly orthogonal orientation with respect to the scaffold, in order to optimally fill the space underneath the hydrophobic glycine-rich loop.

SAR Study. We started the optimization study of compound **1** by varying the substitution pattern on ring A. This investigation was mainly focused on R_3 substituent (see Table 1) at position 2', according to the evaluation deriving from the structural and computational studies previously discussed. In Table 1, the biochemical IC_{50} values (μM) for ALK and for the most critical kinases among the hit ones, i.e., IR (insulin receptor) and its closest family member IGF1R (insulin-like growth factor 1 receptor), are reported along with the antiproliferative activity on the ALK-dependent ALCL Karpas-299 cell line (IC_{50} evaluated after 72 h treatment). Generally, a nearly 10-fold or greater selectivity versus IR and IGF1R is observed for all the compounds. In the toxicological studies performed later on our candidate compound **2**, this selectivity ratio was considered safe based on the experimental determination of glucose and insulin levels.

The introduction of an unsubstituted amino group at R_3 led to compound **4**, which displays an unchanged potency respect to **1**. This was in line with modeling predictions as compound **4** lacks the crucial substituent suitable to fill the sugar pocket.

R_3 aminoaliphatic chains substituted with a methoxy group generally led to a moderate loss in ALK activity (see compounds **5**, **7**, and **8**). At best, activity was conserved (see compound **6**) without any improvement with the exception for the good cellular activity of **6** in the double-digit nanomolar range.

Compounds **9** and **11**, bearing shorter two carbon aliphatic chains decorated with a fluorine and a hydroxyl group, respectively, display a surprisingly good biochemical potency on ALK. Compound **9** also shows good antiproliferative cellular activity ($IC_{50} = 0.049 \mu M$). The data related to **12**, **13**, and **14** suggest that they cannot properly accommodate the *ortho* substituent of ring A within the sugar pocket. Compound **15**, with an aminocyclohexyl ring in R_3 , is poorly active, but when it

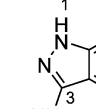
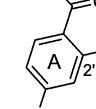
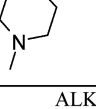
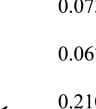
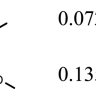
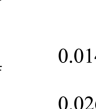
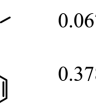
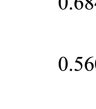
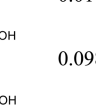
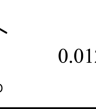
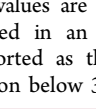
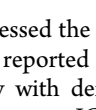
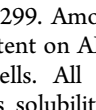
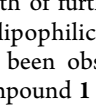
is “decorated” with a hydroxyl group as in **17**, good biochemical and cellular activity are restored. In particular, the trans diastereoisomer **17** is better than the cis one **19** in both enzymatic and cellular assays. The crystal structure of **17** (see Supporting Information, Figure S1) revealed a hydrogen bond interaction mediated by a water molecule of the hydroxyl group with a carbonyl of His1124 in the glycine-rich loop, thus potentially explaining the observed activity of this compound. When R_3 is a 4-amino-N-methylpiperidinyl or a 4-amino-tetrahydropyranyl ring, compounds **20** and **2** display a very good biochemical potency on ALK with IC_{50} values of 0.015 and $0.012 \mu M$, respectively. However, the former showed weak cellular activity, which might be due to low cell permeability, as observed in a Caco-2 permeability experiment (P_{app} A–B = $1.5 \times 10^{-6} \text{ cm/s}$).

Structure–activity relationship (SAR) Tables 2, 3, and 4 show results where the 4-aminotetrahydropyranyl ring was maintained at position 2' of ring A, and the other regions of the structure were modified.

As reported in Table 2, the introduction of a methyl onto linker L afforded a racemic mixture, which upon chiral column chromatography separation yielded enantiomers **26** and **27** whose absolute stereochemistry has not been assigned. The two compounds have a moderately different activity on ALK with **27** showing the best potency. Compared to compound **2**, it displays a stronger activity in cells. However, the labor-intensive chiral separation and the labile nature of the benzhydryl stereogenic center discouraged any further development of this compound.

The exploration of ring B confirmed the contribution of the fluorine interaction with the protein observed in the crystal structure. As depicted in Table 3, removal of both fluorines caused a nearly 10-fold decrease of biochemical activity on ALK and, correspondingly, of antiproliferative activity in Karpas-299 cells (see compound **28**). The presence of a single fluorine as in compound **29** was sufficient to restore the activity on ALK analogously to the introduction of both halogens with the different 2,5-regiochemistry (see compound **30**). Both compounds display an activity profile similar to compound **2**. A decrease in the potency was observed when replacing one fluorine with a methyl group in the 2,5-substituted ring B (see derivative **31**). This substitution is likely to negatively impact the geometry of the stacking interaction of phenyl B with the phenylalanine 1127 of the glycine-rich loop.

Table 1. SAR: Substitution on Ring A (IC_{50} , μM)^a

Cmpd #	R ₃	ALK ^a	IGF1R ^a	IR ^a	Karpas-299 ^b
1	H	0.073	1.441	1.806	0.253
4	NH ₂	0.067	1.335	1.303	0.214
5		0.210	2.112	1.764	0.243
6		0.072	ND	1.069	0.074
7		0.135	ND	1.190	0.194
8		0.099	ND	1.642	0.340
9		0.014	0.271	0.462	0.049
11		0.026	ND	0.906	0.118
12		0.067	0.244	0.353	0.386
13		0.378	ND	3.694	1.259
14		0.684	ND	9.866	0.991
15		0.560	ND	3.822	0.609
17		0.010	0.124	0.189	0.068
19		0.098	0.762	0.707	0.162
20		0.015	0.209	0.330	0.438
2		0.012	0.122	0.209	0.031

^aBiochemical IC_{50} values are reported as the mean ($n \geq 2$). ^b IC_{50} values as determined in an antiproliferative activity assay (72 h treatment) are reported as the mean of 2–3 experiments with a coefficient of variation below 35%.

Finally, we addressed the solubilizing group with variations in the R₄ position as reported in Table 4. All of these compounds compare favorably with derivative 2, in terms of potency on ALK, of selectivity versus IGF1R and IR and of antiproliferative activity in Karpas-299. Among them, analogue 22 was from 3- to 5-fold more potent on ALK than the others and more active on Karpas-299 cells. All of these compounds showed an improved aqueous solubility with respect to 2 (see Table 5) and appeared worth of further study.

In terms of lipophilic ligand efficiency, a significant improvement has been observed for compound 2 compared to the starting compound 1 (see Supporting Information, Table

S2 and Figure S2). It ranges as the second best compound after derivative 22, which, however, is characterized by an unsatisfactory pharmacokinetic profile as discussed below.

On the basis of the in vitro biological data reported in the previous SAR tables, we selected a subset of the most interesting compounds and profiled them for their in vitro absorption, distribution, metabolism, and excretion (ADME) properties, with the aim to anticipate potential liabilities in in vivo studies. The results of this profiling are shown in Table 5, where medium-throughput solubility data at physiological pH, compound permeability evaluation in the Caco-2 cell permeability assay, and intrinsic clearance both in human liver microsomes (HLM) and in rat hepatocytes are reported.

Compounds 21, 22, 23, and 24 display a moderate to good solubility with an improvement relative to 2, as expected. The Caco-2 permeability appears generally low, with compound 21 showing higher B–A P_{app} compared to A–B, while the remaining derivatives show quite similar values. As for the intrinsic clearance in human liver microsomes and in rat hepatocytes, the data range from low to moderate except for 23, which shows a higher value of intrinsic clearance in rat hepatocytes. As the in vitro ADME parameters of the overall compounds were quite similar, we decided to evaluate the pharmacokinetic profile in mouse for all of them and the corresponding data are reported in Table 6.

The mice were treated with the compounds by iv and os administration at the dose of 10 mg/kg. Among them, 9 and 2 clearly emerged as the most interesting derivatives with very high oral bioavailability with low clearance and good volume of distribution and half-life values. The remaining compounds generally display much lower oral bioavailability with low exposure in most cases. However, compound 9 turned out to be less potent in following in vivo efficacy experiments, thus we focused our attention on 2.

Compound 2 Characterization. An in-depth profiling of compound 2 was undertaken, including its potency on both kinase and cellular panels.

The compound has been profiled on a highly diverse panel of 56 biochemical kinase assays (kinase selectivity screening, KSS), and key data are reported in Table 7. We found that compound 2 has an average IC_{50} of 12 nM on the ALK kinase. To better characterize the inhibitor potency on the target, we then calculated a K_i of 6.2 nM, which is in line with the calculated IC_{50} . Compound 2 was even more potent on the kinases ROS1 ($IC_{50} = 0.007 \mu\text{M}$) and on TRKA ($IC_{50} = 0.001 \mu\text{M}$). Only on two additional kinases, JAK2 and ACK1, the compound shows a less than 10-fold selectivity. For 12 additional kinases, a selectivity ratio equal or greater than 10 is observed, while for the other 40 kinases at least a 100-fold selectivity is observed.

On the basis of the observed activity on TRKA, the biochemical potencies on the related kinases TRKB and TRKC were also evaluated and found to be in the single-digit nanomolar range (TRKB $IC_{50} = 0.002 \mu\text{M}$ and TRKC $IC_{50} = 0.005 \mu\text{M}$).

Then compound 2 was profiled on a panel of nearly 200 human tumor cell lines (see Table 8). The antiproliferative activity observed is consistent with the compound kinase selectivity profile, as compound 2 displays an IC_{50} below 0.1 μM on different ALK-dependent cancer cells, such as ALCL cell lines Karpas 299, SU-DHL-1, SUP-M2, and SR-786 and NSCLC cell line NCI-H2228. In addition, it also potently inhibits ($IC_{50} = 0.017 \mu\text{M}$) the proliferation of KM12, a human

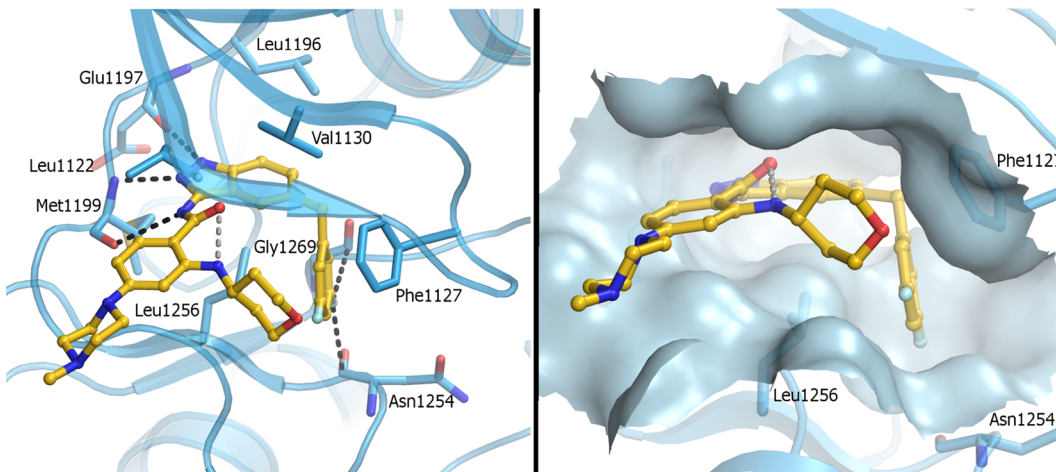
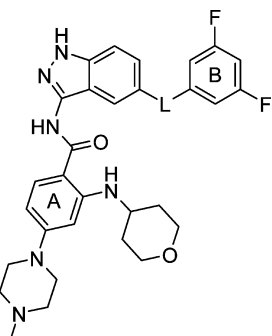


Figure 5. (left) Binding mode of compound 2 (yellow carbon atoms) into the ALK active site (light-blue carbon atoms; PDB 5FTO). The gray dashed line indicates the intramolecular hydrogen bond, whereas black dashed lines represent hydrogen bonds and multipolar interactions. (right) Surface representation of the ALK active site showing the conformation adopted by the tetrahydropyranyl ring.

Table 2. SAR: Linker Modification (IC_{50} , μM)^a



compd no.	L	ALK ^a	IGF1R ^a	IR ^a	Karpas-299 ^b
26 ^c	CHCH ₃	0.059	ND	1.163	0.041
27 ^c	CHCH ₃	0.019	0.136	0.189	0.016
2	CH ₂	0.012	0.122	0.209	0.031

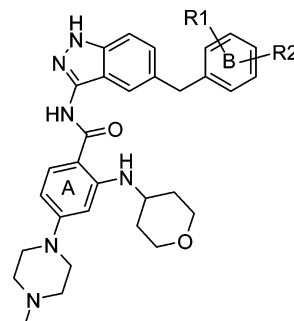
^aBiochemical C_{50} values are reported as the mean ($n \geq 2$). ^b IC_{50} values as determined in an antiproliferative activity assay (72 h treatment) are reported as the mean of 2–3 experiments with a coefficient of variation below 35%. ^cAbsolute configuration unknown.

CRC cell line whose growth was recently found to be TRKA-dependent due to the presence of the oncogenic tropomyosin 3-NTRK1 (TPM3-NTRK1) chromosomal rearrangement,²⁴ whereas the antiproliferative activity observed in MV-4-11 is presumably due to the cross-reactivity with FLT3. The additional not reported IC_{50} s are comprised between 0.1 and 1 μM for 11 cell lines and greater than 1 μM for the remaining cell lines.

In ALK-dependent models the inhibition of cell growth was correlated with the modulation of the activated target in cells. In the ALCL cell line Karpas-299 and in NSCLC cell line NCI-H2228, the ability of the compound to modulate the autophosphorylation of the ALK kinase was assessed after 2 h treatment at different concentrations. As reported in Figure 6, a complete inhibition of ALK phosphorylation can be clearly appreciated in both cell lines at very low doses. Consistently a dose-dependent inhibition of phosphorylation of the downstream effector STAT3 is also clearly observed.

To further explore the cellular activity on TRKA, the modulation of target phosphorylation was also studied on

Table 3. SAR: Substitution Pattern on Ring B (IC_{50} , μM)^a



compd no.	R ₁	R ₂	ALK ^a	IGF1R ^a	IR ^a	Karpas-299 ^b
28	H	H	0.106	0.903	1.489	0.182
29	3-F	H	0.030	0.206	0.427	0.018
30	2-F	5-F	0.038	ND	0.170	0.049
31	2-CH ₃	5-F	0.181	ND	0.823	0.851
2	3-F	5-F	0.012	0.122	0.209	0.031

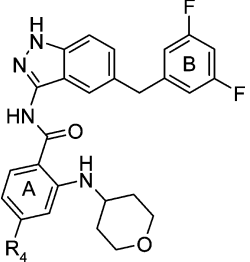
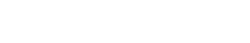
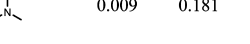
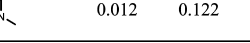
^aBiochemical C_{50} values are reported as the mean ($n \geq 2$). ^b IC_{50} values as determined in an antiproliferative activity assay (72 h treatment) are reported as the mean of 2–3 experiments with a coefficient of variation below 35%.

KM12, a TRKA-dependent cellular model. KM12 cells have been treated for 2 h with compound 2 at different concentrations, and then the phosphorylation of TRKA and downstream transducers has been evaluated. As reported in Figure 7, a clear inhibition of target and signaling pathway phosphorylation is observed at low compound concentration, supporting the rationale for considering TRKA-positive patients for clinical development of compound 2.

To evaluate and compare the inhibition by compound 2 of its main targets in the same cellular environment, the interleukine-3 (IL-3)-dependent Ba/F3 cell line was transfected and made dependent for survival on ALK, ROS1, TRKA, TRKB, and TRKC kinases.³⁴ These IL-3-independent cell lines were treated with compound 2, which has shown the antiproliferative activities reported in Table 9.

Compound 2 proved to be very potent in inhibiting the growth of ALK-, ROS1-, TRKA-, TRKB-, and TRKC-dependent Ba/F3 cell lines with IC_{50} values in the low

Table 4. SAR: Solubilizing Group Variations on Ring A (IC_{50} , μM)^a

Cmpd #	R ₄	ALK ^a	IGF1R ^a	IR ^a	Karpas-299 ^b
21		0.015	0.364	0.457	0.050
22		0.003	0.028	0.041	0.013
23		0.018	0.391	0.653	0.038
24		0.009	0.181	0.196	0.043
2		0.012	0.122	0.209	0.031

^aBiochemical IC_{50} values are reported as the mean ($n \geq 2$). ^b IC_{50} values as determined in an antiproliferative activity assay (72 h treatment) are reported as the mean of 2–3 experiments with a coefficient of variation below 35%.

Table 5. In Vitro ADME Parameters of Selected Derivatives

compd no.	solubility pH 7 (μM)	permeability		intrinsic clearance	
		Caco-2 ^a P_{app} [$10^{-6} cm/s$] (P _{app} B–A)	HLM ^b (mL/min/kg)	rat hepatocytes (mL/min/kg)	intrinsic clearance
21	51	2.7 (19.8)	57	42	
22	103	0.6 (4.5)	7.5	52	
23	84	1.1 (1.9)	40	229	
24	59	0.3 (2)	12	49	
9	16	2.4 (1.5)	24	18	
17	7	1.8 (5.1)	25	45	
2	20	2.4 (3.0)	33	87	

^aCaco-2 permeability assay. ^bHuman liver microsomes.

Table 7. Kinase Profile of Compound 2^a

kinase	IC_{50} (μM)	kinase	IC_{50} (μM)
TRKA	0.001	IGF1R	0.122
TRKB	0.003	FAK	0.140
TRKC	0.005	FLT3	0.164
ROS1	0.007	BRK	0.195
ALK	0.012	IR	0.209
JAK2	0.040	AUR2	0.215
ACK1	0.070	JAK3	0.349
JAK1	0.112	RET	0.393

^aBiochemical IC_{50} values are reported as the mean ($n \geq 2$). They have been calculated using the KSS biochemical panel at 2 Km ATP concentration. $IC_{50} > 1 \mu M$ were obtained for the following kinases: FGFR1, VEGFR2, VEGFR3, LCK, KIT, AUR1, ABL, PKC β , CDK2/CycA, SYK; $IC_{50} > 10 \mu M$ were obtained for: AKT1, CDC7/DBF4, CHK1, CK2, EEF2K, EGFR1, ERK2, GSK3 β , IKK2, MAPKAPK2, MELK, MET, MPS1, MST4, NEK6, NIM1, P38 α , PAK4, PDGFR β , PDK1, PERK, PIM1, PKA α , PLK1, SULU1, ZAP70.

Table 8. Antiproliferative Activity of Compound 2^a (Cell Lines with IC_{50} below 0.1 μM)

cell line	cancer type	IC_{50} (μM) ^a
KM12	adenocarcinoma colon TRKA +	0.017
SU-DHL-1	anaplastic large cell lymphoma ALK +	0.024
KARPAS-299	anaplastic large cell lymphoma ALK +	0.031
SUP-M2	anaplastic large cell lymphoma ALK +	0.041
NCI-H2228	nonsmall cell lung cancer ALK +	0.068
SR-786	anaplastic large cell lymphoma ALK +	0.081
MV-4-11	biphenotypic B myelomonocytic leukemia	0.081

^a IC_{50} values as determined in an antiproliferative activity assay (72 h treatment) are reported as the mean of 2–3 experiments with a coefficient of variation below 35%.

nanomolar range. As expected, compound 2 was poorly active in inhibiting the proliferation of IL-3-dependent Ba/F3 cell line ($IC_{50} = 2.1 \mu M$).

As the emergence of resistance mutations is frequently responsible for relapse in patients treated with ALK inhibitors, we tested compound 2 in a series of Ba/F3 cell lines transfected with different crizotinib or ceritinib-resistant mutated forms of EML4-ALK. Entrectinib demonstrated a good antiproliferative activity on EML4-ALK-wt (Ba/F3-EML4-ALK-wt $IC_{50} = 0.028 \mu M$) and on the gate-keeper mutant EML4-ALK-L1196M (Ba/F3-EML4-ALK-L1196M $IC_{50} = 0.067 \mu M$), but it proved to be poorly active on the EML4-ALK-G1202R mutant (Ba/F3-EML4-ALK-G1202R $IC_{50} = 0.897 \mu M$), as expected based on entrectinib mode of binding.

Table 6. In Vivo ADME Parameters of Selected Derivatives (Harlan nu/nu Mice)^a

compd no.	PK data (iv), dose ^b : 10 mg/kg					PK data (per os), dose ^b : 10 mg/kg				
	C_{max} (μM)	AUC_{∞} ($\mu M \cdot h$)	CL (mL/min/kg)	V_{ss} (L/kg)	$t_{1/2}$ (h)	C_{max} (μM)	T_{max} (h)	AUC_{∞} ($\mu M \cdot h$)	$t_{1/2}$ (h)	F^c (%)
21	10.3 ± 0.1	7.86 ± 0.95	38.8 ± 5.06	4.41 ± 1.30	2.83 ± 1.20	0.081 ± 0.072	6	1.33 ± 0.79	9.63 ± 3.92	2.9
22	40.5 ± 8.85	42.2 ± 6.56	7.01 ± 1.08	1.40 ± 0.41	4.76 ± 0.78	0.36 ± 0.13	0.83 ± 0.29	1.51 ± 0.35	2.25 ± 0.43	18
23	5.69 ± 0.37	7.97 ± 1.04	32.1 ± 3.75	2.63 ± 0.12	1.52 ± 0.09	0.80 ± 0.05	6	11.0 ± 0.21	4.08 ± 0.37	29.3
24	6.93 ± 0.92	33.1 ± 0.72	8.16 ± 0.31	2.62 ± 0.40	4.94 ± 0.63	1.88 ± 0.40	4.33 ± 2.89	31.5 ± 3.99	9.86 ± 1.77	99
9	7.58 ± 1.19	24.7 ± 2.17	11.7 ± 0.87	4.76 ± 0.82	5.92 ± 0.33	0.36 ± 0.38	1	1.25 ± 1.01 ^d		7.3
17	7.06 ± 1.67	13.1 ± 3.32	21.3 ± 4.69	3.02 ± 1.21	3.01 ± 1.32	1.33 ± 0.19	2.5 ± 3.04	17.4 ± 0.21	2.94 ± 0.10	77
2	4.90 ± 1.35	19.6 ± 1.5	13.5 ± 1.05	3.34 ± 0.60	3.59 ± 0.47					

^a $n = 6$ animals per study. ^bDosed in 10% Tween 80/saline iv = intravenous adm.; dosed in 0.5% methocel suspension per os = oral adm.

^cBioavailability. ^dDetectable concentration of the compound were measured up to 6 h post dosing.

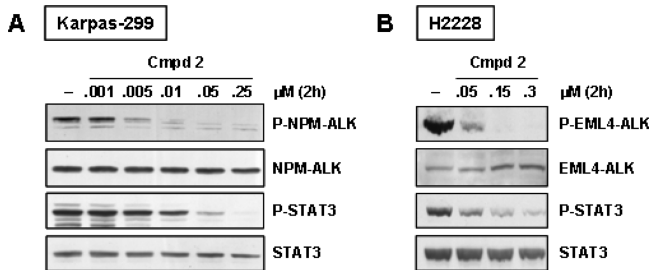


Figure 6. Mechanism of action of compound 2 in Karpas-299 (A) and NCI-H2228 (B) cell lines. Cells were treated with the compound at the indicated concentrations for 2 h, and the levels of P-ALK and P-STAT3 were evaluated by Western blot analysis of cell lysates using specific antibodies.

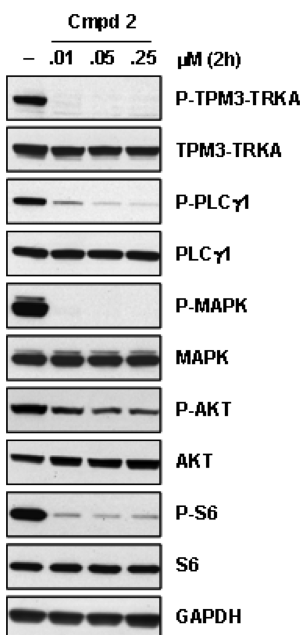


Figure 7. Mechanism of action of compound 2 in KM12 cell line. Cells were treated with the compound at the indicated concentrations for 2 h, and the levels of P-TPM3-TRKA and of phosphorylated downstream transducers were evaluated by Western blot analysis of cell lysates using specific antibodies.

Table 9. Antiproliferative Activity of Compound 2 on Ba/F3 Cells Dependent on ALK, ROS1, and TRKs Kinases

cell line	IC ₅₀ (μM) ^a
Ba/F3	2.104
Ba/F3_ALK	0.028
Ba/F3_ROS1	0.005
Ba/F3_TRKA	0.003
Ba/F3_TRKB	0.003
Ba/F3_TRKC	0.003

^aIC₅₀ values as determined in an antiproliferative activity assay (72 h treatment) are reported as the mean of 2–3 experiments with a coefficient of variation below 35%.

Compound 2 was tested for evaluating its in vivo efficacy in different ALK-dependent tumor models. In the experiment reported in Figure 8, severe combined immune deficiency (SCID) mice bearing Karpas-299 xenograft tumors were treated orally with the compound at the doses of 30 and 60 mg/kg twice a day for 10 consecutive days. Excellent efficacy

was observed at both doses with complete tumor regression achieved at the end of treatment at the dose of 60 mg/kg. At day 90, four out of seven mice treated at the highest dose were still tumor free and were considered cured. No body weight loss or other signs of toxicity were observed in treated animals.

The ex vivo target modulation was evaluated by Western blot analysis after single administration of the compound at the dose of 60 mg/kg to tumor bearing mice. As shown in Figure 8, NPM-ALK and STAT3 phosphorylation is completely inhibited 12 h after compound administration and is still evident at 18 h.

The in vivo efficacy of compound 2 was then evaluated in the ALK-dependent NSCLC NCI-H2228 xenograft model. In the experiment reported in Figure 9, the compound was administered orally at the doses of 30 and 60 mg/kg twice a day for 10 consecutive days to nude mice bearing NCI-H2228 xenograft tumors. At both doses, complete tumor regression was observed in all the animals at the end of treatment. The in vivo target modulation was also evaluated in this ALK-dependent NSCLC model. In Figure 9, the complete inhibition of EML4-ALK and AKT phosphorylation can be clearly appreciated by Western blot analysis of tumors harvested 12 or 18 h after single oral administration. Because, as mentioned above, low BBB penetration is the major weakness of crizotinib and development of brain metastases is an important cause of relapse in crizotinib-treated patients, we decided to investigate the ability of compound 2 to cross the BBB. The value of brain levels measured after oral administration of the compound to nu/nu mice reaches nearly 50% of plasma levels, as reported in Table 10. Such brain levels suggest the possibility to reach an efficacious exposure of the compound also in the brain.

To further characterize compound 2, its pharmacokinetic parameters in rat and dog have been evaluated by treating the animals at the dose of 10 mg/kg for both iv and oral administration as reported in Table 11. Good exposure and moderate to good oral bioavailability have been reached in both species, with volume of distribution indicative of tissue distribution and low clearance in both animal species. This profile allowed the evaluation of the safety and tolerability of this compound in further animal studies.

CONCLUSIONS

In conclusion, we have identified a novel 3-aminoindazole ALK inhibitor (compound 2) through the optimization of the starting hit compound 1. Compound 2 is a potent ALK, ROS1, and TRKs inhibitor with nanomolar activity on the corresponding target-driven cell lines. It shows a favorable pharmacokinetic profile in rodent and nonrodent animal species, and it induces stable tumor regression in ALK-dependent ALCL and NSCLC human xenograft tumor models with a clear inhibition of ALK and downstream effector phosphorylation. Compound 2, based on its permissive safety and tolerability profile, was selected for development, and it is currently undergoing phase I/II clinical trials for the treatment of patients affected by ALK-, ROS1-, and TRKs-dependent tumors with remarkable signs of activity.^{29,30} An exhaustive biological and pharmacological profile of compound 2, including its activity on a panel of resistant mutants identified in patients treated with different ALK inhibitors, is under publication.³⁵

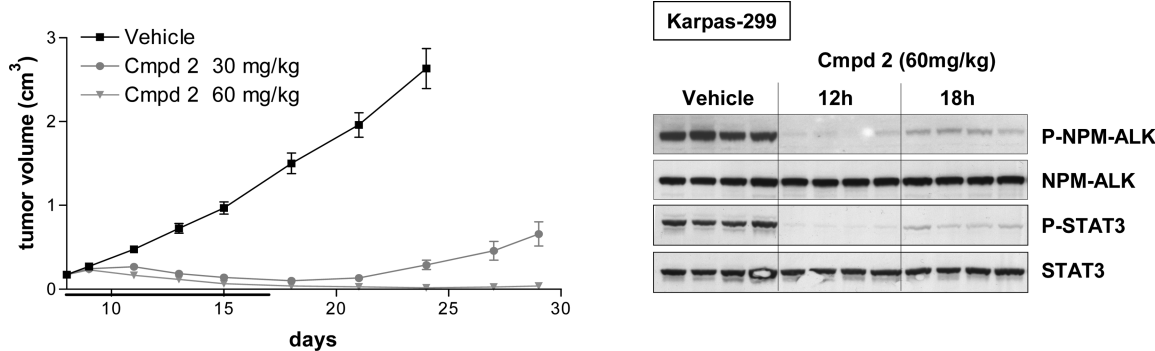


Figure 8. In vivo efficacy of compound 2 in Karpas 299 ALK-dependent xenograft model and ex vivo target modulation. (left) Nu/Nu mice bearing established Karpas-299 tumors were treated with compound 2 at the doses of 30 and 60 mg/kg per os twice a day for 10 consecutive days. (right) To evaluate ex vivo target modulation, mice were administered a single dose of 60 mg/kg and sacrificed 12 h or 18 h after the treatment. Levels of P-NPM-ALK and P-STAT3 in tumor lysates were analyzed by Western blot using specific antibodies.

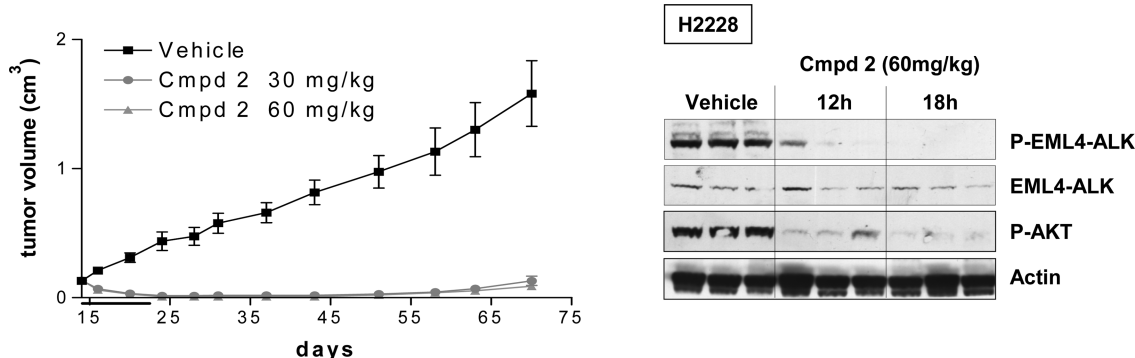


Figure 9. In vivo efficacy of compound 2 in NSCLC NCI-H2228 ALK-dependent xenograft model and ex vivo target modulation. (left) Nu/Nu mice bearing established NCI-H2228 tumors were treated with compound 2 at the doses of 30 and 60 mg/kg per os twice a day for 10 consecutive days. (right) To evaluate ex vivo target modulation mice were administered a single dose of 60 mg/kg and sacrificed 12 h or 18 h after the treatment. Levels of P-EML4-ALK and P-STAT3 in tumor lysates were analyzed by Western blot using specific antibodies.

Table 10. Brain and Plasma Levels of Compound 2 after 2-Week Repeated Administration in Mouse

species	treatment	dose	plasma levels	brain levels	brain/plasma
mouse	2 weeks	240 mg/kg/day	4.57 μM	1.94 μM	0.43

EXPERIMENTAL SECTION

1. Chemistry. Unless otherwise noted, solvents and reagents were obtained from commercial suppliers and used without further purification. All reactions involving air- or moisture-sensitive reagents were performed under an argon atmosphere. All final compounds were purified to >95% purity as determined by high-performance liquid chromatography (HPLC). HPLC-MS/UV analyses were performed on a LCQ DecaXP (Thermo, San Jose, US) ion trap instrument, equipped with an electrospray (ESI) ion source. The mass spectrometer is connected to a Surveyor HPLC system (Thermo, San Jose, US) with an UV photodiode array detector (UV detection

215–400 nm). A Waters XSelect CSH C18 column 50 × 4.6 mm, 3.5 μm particle size, was used. Mobile phase A was ammonium acetate 5 mM buffer (pH 4.5 with acetic acid):acetonitrile 95:5, and mobile phase B was ammonium acetate 5 mM buffer (pH 4.5 with acetic acid):acetonitrile 5:95. Gradient from 0 to 100% B in 7 min, hold 100% B 2 min. Flow rate 1 mL/min. Injection volume 10 μL. Full scan, mass range from 50 to 1200 amu. Heated capillary temp was 275 °C, and spray voltage value was set at 4 kV. Mass are given as *m/z* ratio. Instrument control, data acquisition, and processing were performed by using Xcalibur 1.2 software (Thermo). Column chromatography was conducted either under medium pressure on silica gel (Merck silica gel 40–63 μm) or on prepacked silica gel cartridges (Biotage) on a Horizon system. ¹H NMR spectra were acquired at 25 °C in DMSO-*d*₆ on a Varian Inova 400 spectrometer operating at 400 MHz and equipped with a 5 mm ¹H{¹⁵N-³¹P} Z-axis-PFG indirect detection probe. Residual not-deuterated solvent signal was used as reference with δ = 2.50 ppm for DMSO-*d*₆. Data are reported as follows: chemical shift, multiplicity (s = singlet, d = doublet, t = triplet, q = quartet, quint = quintet, bs = broad singlet, bd = broad doublet, dd = doublet of doublet, td = triplet of doublet, m =

Table 11. Pharmacokinetic Profile of Compound 2 in Rat (Sprague Dawley Rats)^a and Dog (Beagle Dog)^b

species	PK data (iv), dose: ^c 10 mg/kg					PK data (per os), dose: ^c 10 mg/kg				
	C _{max} (μM)	AUC _∞ (μM·h)	CL (mL/min/kg)	V _{ss} (L/kg)	t _{1/2} (h)	C _{max} (μM)	T _{max} (h)	AUC _∞ (μM·h)	t _{1/2} (h)	F (%) ^d
rat	11.0 ± 1.1	15.1 ± 1.5	20.8 ± 2.1	4.0 ± 0.4	3.5 ± 0.3	0.5 ± 0.1	3.08	5.13 ± 0.18	3.8 ± 0.2	43 ^e
dog	8.6 ± 2.5	17.6 ± 3	17.5 ± 3.6	6.7 ± 0.9	11.9 ± 6.0	0.6 ± 0.2	2.0	5.7 ± 2.6	15.2 ± 8.9	32

^an = 6 animals per study. ^bn = 3 animals per study. ^cDosed in 10% Tween 80/saline iv = intravenous administration; dosed in 0.5% methocel suspension per os = oral administration. ^dBioavailability. ^eF % calculated based on the actual 8 mg/kg oral dose.

multiplet), coupling constants, and number of protons. As formerly reported,³⁶ ESI(+) high-resolution mass spectra (HRMS) were obtained on a Q-Tof Ultima (Waters, Manchester, UK) mass spectrometer directly connected with a Agilent 1100 micro-HPLC system (Palo Alto, CA, US). Thin-layer chromatography was performed on Merck silica gel 60 plates coated with 0.25 mm layer with fluorescent indicator. Components were visualized by UV light ($\lambda = 254$ and 366 nm) and iodine vapors.

Synthesis of Scaffold I and II. General Procedure for Diarylmethanes Preparation. 3-Cyano-4-fluorophenylboronic acid (1 equiv), powdered K₃PO₄ (2 equiv), and Pd(PPh₃)₄ (2% mol) were charged in an oven-dried flask under argon atmosphere. The flask was evacuated and backfilled with argon three times. Toluene (3 mL/mmol boronic acid) and benzyl bromide (1 equiv) were added under good stirring. The reaction mixture was heated to 100 °C in half an hour and maintained at that temperature for 1.5–8 h. The dark mixture was taken up with diethyl ether, washed with saturated aqueous NH₄Cl, and brine. The organic phase was dried over anhydrous Na₂SO₄ and evaporated to dryness. The residue was then purified by flash chromatography (*n*-hexane/ethyl acetate) to provide the desired diarylmethane in yields of 60–90%.

General Procedure for 3-Aminoindazoles Preparation. A mixture of 3-cyano-4-fluoro-diarylmethane (1 equiv) and hydrazine hydrate (5 equiv) in *n*-butanol (2.5 mL/mmol diarylmethane) was refluxed overnight. The reaction mixture was diluted with water/ethyl acetate, and the organic phase was washed twice with brine, dried, and evaporated. The residue was purified by flash chromatography (CH₂Cl₂/EtOH) to provide the desired 3-aminoindazole in yields of 75–90%.

General Procedure for Diarylmethanes Alkylation. A mixture of 3-cyano-4-fluoro-diarylmethane (1 equiv) and methyl iodide (1.5 equiv) was dissolved in THF dry (8 mL/mmol diarylmethane) under nitrogen atmosphere at –20 °C. Bis(trimethylsilyl)-lithiumamid 1.0 M in THF (2 equiv) was gradually added. After 20 min, the reaction was quenched by adding a solution of KHSO₄ 10% and extracted with ethyl acetate. The organic phase was washed with aqueous KHSO₄ 10% and brine, dried over sodium sulfate, and evaporated to dryness. The crude was purified by flash chromatography (hexane/ethyl acetate) to provide the desired alkylated diarylmethane in yields of 70–85%.

Synthesis of 3-acyl-5-benzyl indazoles 2, 3, 5–10, 12–16, 18, 20–25, and 28–31.

N-[5-(3,5-Difluoro-benzyl)-1H-indazol-3-yl]-4-(4-methyl-piperazin-1-yl)-2-(tetrahydro-pyan-4-ylamino)-benzamide (2). To a suspension of 4-(4-methyl-piperazin-1-yl)-2-[(tetrahydro-pyan-4-yl)-(2,2,2-trifluoro-acetyl)-amino]-benzoic acid trifluoroacetate (10 g, 22.1 mmol) in dry dichloromethane (300 mL), oxalyl chloride (3.58 mL, 42.3 mmol) and *N,N*-dimethylformamide (1–2 drops) were added. The mixture was stirred at room temperature for 2 h then evaporated to dryness. The resulting crude acyl chloride was taken-up with toluene, evaporated, and then dissolved in dry tetrahydrofuran (130 mL) at –20 °C. A solution of 5-(3,5-difluoro-benzyl)-1H-indazol-3-ylamine (5 g, 19.28 mmol) and *N,N*-diisopropylethylamine (12.8 mL, 73.3 mmol) in dry THF (40 mL) was added to the cooled reaction mixture. The mixture was stirred at –20 °C for 4 h then quenched by adding water/ethyl acetate. The organic phase was washed with a saturated solution of sodium hydrogenocarbonate, dried over sodium sulfate, and evaporated to dryness.

Crude reaction mixture is dissolved in methanol (375 mL) in the presence of triethylamine (60 mL) and stirred at 65 °C for 2 h. The solvents were removed under reduced pressure and the residue treated with water/ethyl acetate. Organic phase was dried over sodium sulfate and evaporated to dryness. Purification of the crude by chromatography over silica gel (DCM/EtOH/NH₃, 5 N in MeOH = 1000/50/S) and crystallization of the so obtained compound from ethyl acetate/hexane afforded 8.4 g of the title compound as a white solid (78% yield).

¹H NMR (400.5 MHz, DMSO-*d*₆) δ ppm 1.29–1.41 (m, 2H) 1.89–1.97 (m, 2H) 2.24 (s, 3 H) 2.41–2.48 (m, 4H) 3.23–3.29 (m, 4 H) 3.49 (ddd, *J* = 11.7, 10.2, 2.3 Hz, 2 H) 3.62–3.72 (m, 1 H) 3.80

(ddd, *J* = 11.7, 3.8, 3.8 Hz, 2 H) 4.04 (s, 2 H) 6.13 (d, *J* = 2.1 Hz, 1 H) 6.23 (dd, *J* = 9.0, 2.2 Hz, 1 H) 6.93–7.04 (m, 3 H) 7.25 (dd, *J* = 8.7, 1.5 Hz, 1 H) 7.40 (d, *J* = 8.7 Hz, 1 H) 7.48 (s, 1 H) 7.80 (d, *J* = 9.0 Hz, 1 H) 8.29 (d, *J* = 7.6 Hz, 1 H) 10.07 (s, 1 H) 12.62 (s, 1 H). LCMS (ESI) *m/z* 507 (M + H)⁺. HRMS (ESI) calcd for C₃₁H₃₄F₂N₆O₂ + H⁺ 561.2784, found 561.2785.

By employing the above-described procedure, starting from scaffold I or II and benzoic acid III², the following compounds were prepared.

N-[5-(3,5-Difluoro-benzyl)-1H-indazol-3-yl]-2-nitro-benzamide (3). Eluant for column chromatography: DCM/EtOH/NH₃, 5 N in MeOH = 100/5/1. ¹H NMR (400.5 MHz, DMSO-*d*₆) δ ppm 2.23 (s, 3 H) 2.42–2.47 (m, 4 H) 3.33–3.38 (m, 4 H) 4.05 (s, 2 H) 7.01 (tt, *J* = 9.4, 2.4 Hz, 2H) 7.24 (dd, *J* = 8.7, 1.6 Hz, 1 H) 7.27 (br s, 1 H) 7.41 (d, *J* = 8.7 Hz, 1 H) 7.44 (br s, 1 H) 7.63 (s, 1 H) 7.69 (br s, 1 H) 10.81 (br s, 1 H) 12.70 (s, 1 H). LCMS (ESI) *m/z* 561 (M + H)⁺. HRMS (ESI) calcd for C₂₆H₂₄F₂N₆O₃ + H⁺ 507.1951, found 507.1947.

N-[5-(3,5-Difluoro-benzyl)-1H-indazol-3-yl]-2-(2-methoxy-ethylamino)-4-(4-methyl-piperazin-1-yl)-benzamide (5). Eluant for column chromatography: DCM/EtOH/NH₃, 5 N in MeOH = 100/5/1. ¹H NMR (400.5 MHz, DMSO-*d*₆) δ ppm 2.25 (s, 3 H) 2.44–2.49 (m, 4 H) 3.26 (s, 3 H) 3.27–3.31 (m, 6 H) 3.54 (t, *J* = 5.5 Hz, 2 H) 4.05 (s, 2 H) 6.09 (d, *J* = 1.9 Hz, 0 H) 6.25 (dd, *J* = 9.0, 1.9 Hz, 0 H) 6.94–7.04 (m, 3 H) 7.24 (dd, *J* = 8.7, 1.6 Hz, 1 H) 7.41 (d, *J* = 8.7 Hz, 1H) 7.51 (s, 1 H) 7.79 (d, *J* = 9.0 Hz, 1 H) 8.23 (t, *J* = 4.9 Hz, 1 H) 10.06 (s, 1 H) 12.63 (s, 1 H). LCMS (ESI) *m/z* 535 (M + H)⁺. HRMS (ESI) calcd for C₂₉H₃₂F₂N₆O₂ + H⁺ 535.2628, found 535.2632.

N-[5-(3,5-Difluoro-benzyl)-1H-indazol-3-yl]-2-((R)-2-methoxy-1-methyl-ethylamino)-4-(4-methyl-piperazin-1-yl)-benzamide (6). Eluant for column chromatography: DCM/EtOH/NH₃, 5 N in MeOH = 100/10/1. ¹H NMR (400.5 MHz, DMSO-*d*₆) δ ppm 1.14 (d, *J* = 6.3 Hz, 3 H) 2.23 (s, 3 H) 2.41–2.47 (m, 4 H) 3.24–3.29 (m, 4 H) 3.27 (s, 3 H) 3.30–3.40 (m, 2 H) 3.74–3.83 (m, 1 H) 4.05 (s, 2 H) 6.13 (d, *J* = 2.2 Hz, 1 H) 6.24 (dd, *J* = 9.0, 2.2 Hz, 1 H) 6.94–7.04 (m, 3 H) 7.25 (dd, *J* = 8.7, 1.6 Hz, 1 H) 7.41 (d, *J* = 8.7 Hz, 1 H) 7.49 (s, 1 H) 7.78 (d, *J* = 9.0 Hz, 1 H) 8.20 (d, *J* = 7.7 Hz, 1 H) 10.04 (s, 1 H) 12.63 (s, 1 H). LCMS (ESI) *m/z* 549 (M + H)⁺. HRMS (ESI) calcd for C₃₀H₃₄F₂N₆O₂ + H⁺ 549.2784, found 549.2787.

N-[5-(3,5-Difluoro-benzyl)-1H-indazol-3-yl]-2-(3-methoxy-propylamino)-4-(4-methyl-piperazin-1-yl)-benzamide (7). Eluant for column chromatography: DCM/EtOH/NH₃, 5 N in MeOH = 100/5/1. ¹H NMR (400.5 MHz, DMSO-*d*₆) δ ppm 1.79 (quin, *J* = 6.5 Hz, 2 H) 2.22 (s, 3 H) 2.41–2.46 (m, 4 H) 3.17 (q, *J* = 6.5 Hz, 2 H) 3.21 (s, 3 H) 3.25–3.31 (m, 4 H) 3.40 (t, *J* = 6.5 Hz, 2 H) 4.03 (s, 2 H) 6.05 (d, *J* = 2.2 Hz, 1H) 6.23 (dd, *J* = 9.0, 2.2 Hz, 1 H) 6.93–7.03 (m, 3 H) 7.23 (dd, *J* = 8.7, 1.6 Hz, 1 H) 7.40 (d, *J* = 8.6 Hz, 1 H) 7.50 (s, 1 H) 7.79 (d, *J* = 9.0 Hz, 1 H) 8.18 (t, *J* = 5.2 Hz, 1 H) 10.06 (s, 1 H) 12.61 (s, 1 H). LCMS (ESI) *m/z* 549 (M + H)⁺. HRMS (ESI) calcd for C₃₀H₃₄F₂N₆O₂ + H⁺ 549.2784, found 549.2780.

N-[5-(3,5-Difluoro-benzyl)-1H-indazol-3-yl]-2-(2-methoxy-1-methoxymethyl-ethylamino)-4-(4-methyl-piperazin-1-yl)-benzamide (8). Eluant for column chromatography: DCM/MeOH/NH₃, 5 N in MeOH = 100/5/1. ¹H NMR (400.5 MHz, DMSO-*d*₆) δ ppm 2.42 (br s, 3 H) 2.70 (br s, 4 H) 3.18–3.44 (m, 4 H) 3.26 (s, 6 H) 3.41 (d, *J* = 5.0 Hz, 4 H) 3.80–3.88 (m, 1 H) 4.04 (s, 2 H) 6.20 (d, *J* = 2.1 Hz, 1 H) 6.26 (dd, *J* = 8.9, 2.1 Hz, 1 H) 6.94–7.03 (m, 3 H) 7.24 (dd, *J* = 8.9, 1.5 Hz, 1 H) 7.41 (d, *J* = 8.7 Hz, 1 H) 7.48 (s, 1 H) 7.79 (d, *J* = 8.9 Hz, 1 H) 8.32 (d, *J* = 8.3 Hz, 1 H) 10.06 (s, 1 H) 12.64 (s, 1 H). LCMS (ESI) *m/z* 579 (M + H)⁺. HRMS (ESI) calcd for C₃₁H₃₆F₂N₆O₃ + H⁺ 579.2890, found 579.2890.

N-[5-(3,5-Difluoro-benzyl)-1H-indazol-3-yl]-2-(2-fluoro-ethylamino)-4-(4-methyl-piperazin-1-yl)-benzamide (9). Eluant for column chromatography: DCM/MeOH = 95/5. ¹H NMR (400.5 MHz, DMSO-*d*₆) δ ppm 2.24 (s, 3 H) 2.43–2.48 (m, 4 H) 3.26–3.31 (m, 4 H) 3.48 (ddt, *J*_{HF} = 27.7, *J*_{HH} = 5.4, 4.9, 4.9 Hz, 2 H) 4.04 (s, 2 H) 4.60 (dt, *J*_{HF} = 47.7, *J*_{HH} = 4.9, 4.9 Hz, 2 H) 6.12 (d, *J* = 2.2 Hz, 1 H) 6.27 (dd, *J* = 9.0, 2.2 Hz, 1 H) 6.94–7.04 (m, 3 H) 7.23 (dd, *J* = 8.5, 1.6 Hz, 1 H) 7.40 (d, *J* = 8.5 Hz, 1 H) 7.50 (s, 1 H) 7.80 (d, *J* = 9.0 Hz, 1 H) 8.36 (t, *J* = 5.4 Hz, 1 H) 10.10 (s, 1 H) 12.62 (s, 1 H). LCMS (ESI)

m/z 523 ($M + H$)⁺. HRMS (ESI) calcd for $C_{28}H_{29}F_3N_6O + H^+$ 523.2428, found 523.2427.

*2-[{2-[{tert-Butyl(dimethylsilyl)oxy}ethyl]amino}-N-[5-(3,5-difluorobenzyl)-1*H*-indazol-3-yl]-4-(4-methylpiperazin-1-yl)-benzamide (10).* ESI(+) MS: *m/z* 635 ($M + H$)⁺.

*N-[5-(3,5-Difluorobenzyl)-1*H*-indazol-3-yl]-2-[{(1-methylazetidin-3-yl)methyl]amino}-4-(4-methylpiperazin-1-yl)-benzamide (12).* Eluant for column chromatography: DCM/MeOH/NH₃ 5 N in MeOH = 100/10/1. ¹H NMR (400.5 MHz, DMSO-*d*₆) δ ppm 2.25 (s, 3 H) 2.43–2.48 (m, 4 H) 2.62 (br s, 3 H) 2.85–2.95 (m, 1 H) 3.31 (m overlapped by water signal, 4 H) 3.37–3.42 (m, 2 H) 3.57 (br s, 2 H) 3.80–3.90 (m, 2 H) 4.03 (s, 2 H) 6.08 (d, *J* = 2.1 Hz, 1 H) 6.27 (dd, *J* = 8.9, 2.1 Hz, 1 H) 6.93–6.99 (m, 2 H) 6.99–7.05 (m, 1 H) 7.24 (dd, *J* = 8.5, 1.5 Hz, 1 H) 7.40 (d, *J* = 8.6 Hz, 1 H) 7.49 (s, 1 H) 7.81 (d, *J* = 8.9 Hz, 1 H) 8.24 (t, *J* = 5.2 Hz, 1 H) 10.11 (s, 1 H) 12.63 (s, 1 H). LCMS (ESI) *m/z* 560 ($M + H$)⁺. HRMS (ESI) calcd for $C_{31}H_{35}F_2N_7O + H^+$ 560.2944, found 560.2954.

*2-Benzylamino-N-[5-(3,5-difluoro-benzyl)-1*H*-indazol-3-yl]-4-(4-methyl-piperazin-1-yl)-benzamide (13).* Eluant for column chromatography: DCM/EtOH/NH₃ 5 N in MeOH = 100/5/1. ¹H NMR (400.5 MHz, DMSO-*d*₆) δ ppm 2.21 (s, 3 H) 2.36–2.44 (m, 4 H) 3.19–3.24 (m, 2 H) 4.03 (s, 2 H) 4.38 (d, *J* = 5.6 Hz, 2 H) 6.08 (d, *J* = 2.2 Hz, 1 H) 6.25 (dd, *J* = 9.0, 2.2 Hz, 1 H) 6.92–7.03 (m, 3 H) 7.21–7.27 (m, 2 H) 7.30–7.36 (m, 2 H) 7.35–7.38 (m, 2 H) 7.39 (d, *J* = 8.5 Hz, 1 H) 7.50 (s, 1 H) 7.80 (d, *J* = 9.0 Hz, 1 H) 8.59 (t, *J* = 5.6 Hz, 1 H) 10.10 (s, 1 H) 12.62 (s, 1 H). LCMS (ESI) *m/z* 567 ($M + H$)⁺. HRMS (ESI) calcd for $C_{33}H_{35}F_2N_6O + H^+$ 567.2679, found 567.2680.

*N-[5-(3,5-Difluoro-benzyl)-1*H*-indazol-3-yl]-4-(4-methyl-piperazin-1-yl)-2-phenylamino-benzamide (14).* Eluant for column chromatography: DCM/EtOH/NH₃ 5 N in MeOH = 100/5/1. ¹H NMR (400.5 MHz, DMSO-*d*₆) δ ppm 2.23 (s, 3 H) 2.46 (br s, 4 H) 3.18–3.24 (m, 4 H) 4.04 (s, 2 H) 6.52 (dd, *J* = 9.0, 2.2 Hz, 1 H) 6.73 (d, *J* = 2.2 Hz, 1 H) 6.93–7.02 (m, 4 H) 7.16–7.20 (m, 2 H) 7.24 (dd, *J* = 8.6, 1.5 Hz, 1 H) 7.28–7.34 (m, 2 H) 7.41 (d, *J* = 8.6 Hz, 1 H) 7.54 (s, 1 H) 7.90 (d, *J* = 9.0 Hz, 1 H) 10.02 (s, 1 H) 10.38 (s, 1 H) 12.68 (s, 1 H). LCMS (ESI) *m/z* 553 ($M + H$)⁺. HRMS (ESI) calcd for $C_{32}H_{30}F_2N_6O + H^+$ 553.2522, found 553.2499.

*2-Cyclohexylamino-N-[5-(3,5-difluoro-benzyl)-1*H*-indazol-3-yl]-4-(4-methyl-piperazin-1-yl)-benzamide (15).* Eluant for column chromatography: DCM/EtOH/NH₃ 5 N in MeOH = 100/5/1. ¹H NMR (400.5 MHz, DMSO-*d*₆) δ ppm 1.16–1.30 (m, 3 H) 1.33–1.45 (m, 2 H) 1.48–1.58 (m, 1 H) 1.57–1.69 (m, 2 H) 1.83–1.92 (m, 2 H) 2.24 (s, 3 H) 2.41–2.48 (m, 4 H) 3.22–3.27 (m, 4 H) 3.40–3.52 (m, 1 H) 4.03 (s, 2 H) 6.08 (d, *J* = 2.1 Hz, 1 H) 6.21 (dd, *J* = 9.0, 2.1 Hz, 1 H) 6.93–7.03 (m, 3 H) 7.25 (dd, *J* = 8.7, 1.6 Hz, 1 H) 7.40 (d, *J* = 8.6 Hz, 1 H) 7.48 (s, 1 H) 7.77 (d, *J* = 9.0 Hz, 1 H) 8.27 (d, *J* = 7.8 Hz, 1 H) 10.04 (s, 1 H) 12.61 (s, 1 H). LCMS (ESI) *m/z* 559 ($M + H$)⁺. HRMS (ESI) calcd for $C_{32}H_{36}F_2N_6O + H^+$ 559.2992, found 559.2992.

*trans-4-{[2-{[5-(3,5-Difluorobenzyl)-1*H*-indazol-3-yl]carbamoyl}-5-(4-methylpiperazin-1-yl)phenyl]amino}cyclohexyl Benzoate (16).* ESI(+) MS: *m/z* 679 ($M + H$)⁺.

*cis-4-{[2-{[5-(3,5-Difluorobenzyl)-1*H*-indazol-3-yl]carbamoyl}-5-(4-methylpiperazin-1-yl)phenyl]amino}cyclohexyl Benzoate (18).* ESI(+) MS: *m/z* 679 ($M + H$)⁺.

*N-[5-(3,5-Difluorobenzyl)-1*H*-indazol-3-yl]-4-(4-methylpiperazin-1-yl)-2-[(1-methylpiperidin-4-yl)amino]benzamide (20).* Eluant for column chromatography: DCM/MeOH/NH₃ 5 N in MeOH = 100/10/1. ¹H NMR (400.5 MHz, DMSO-*d*₆) δ ppm 1.35–1.48 (m, 2 H) 1.87–1.97 (m, 2 H) 2.18 (br s, 3 H) 2.21 (br s, 2 H) 2.23 (s, 3 H) 2.41–2.46 (m, 4 H) 2.61 (br s, 2 H) 3.22–3.27 (m, 4 H) 3.45 (br s, 1 H) 4.04 (s, 2 H) 6.08 (d, *J* = 2.0 Hz, 1 H) 6.22 (dd, *J* = 9.0, 2.0 Hz, 1 H) 6.94–7.03 (m, 3 H) 7.24 (dd, *J* = 8.6, 1.5 Hz, 1 H) 7.40 (d, *J* = 8.5 Hz, 1 H) 7.49 (s, 1 H) 7.78 (d, *J* = 9.0 Hz, 1 H) 8.26 (d, *J* = 7.4 Hz, 1 H) 10.06 (s, 1 H) 12.62 (s, 1 H). LCMS (ESI) *m/z* 574 ($M + H$)⁺. HRMS (ESI) calcd for $C_{32}H_{35}F_2N_7O + H^+$ 574.3101, found 574.3099.

*N¹-[5-(3,5-Difluorobenzyl)-1*H*-indazol-3-yl]-N⁴-[2-(dimethylamino)ethyl]-N⁴-methyl-2-(tetrahydro-2*H*-pyran-4-ylamino)benzene-1,4-dicarboxamide (21).* Eluant for column chromatography: DCM/EtOH/NH₃ 5 N in MeOH = 100/10/1. ¹H NMR (400.5 MHz, DMSO-*d*₆) δ ppm 1.31–1.42 (m, 2 H) 1.87–1.95

(m, 2 H) 2.04 (br s, 3.25 H, rotamer) 2.24 (br s, 2.75 H, rotamer) 2.39 (br s, 1.08 H, rotamer) 2.50 (overlapped by ^{13}C DMSO-*d*₆ signal, 0.92 H, rotamer) 2.91 (br s, 1.38 H, rotamer) 2.97 (br s, 1.63 H, rotamer) 3.31 (overlapped by water signal, 1.08 H, rotamer) 3.45–3.52 (m, 2 H) 3.54 (br s, 0.92 H, rotamer) 3.62–3.72 (m, 1 H) 3.79–3.85 (m, 2 H) 4.05 (s, 2 H) 6.55 (d, *J* = 7.9 Hz, 1 H) 6.75 (s, 1 H) 6.94–7.04 (m, 3 H) 7.27 (dd, *J* = 8.6, 1.6 Hz, 1 H) 7.43 (d, *J* = 8.6 Hz, 1 H) 7.53 (s, 1 H) 7.92 (d, *J* = 7.9 Hz, 1 H) 7.95 (d, *J* = 7.7 Hz, 1 H) 10.55 (s, 1 H) 12.74 (s, 1 H). LCMS (ESI) *m/z* 591 ($M + H$)⁺. HRMS (ESI) calcd for $C_{32}H_{36}F_2N_6O_3 + H^+$ 591.2890, found 591.2891.

*N-[5-(3,5-Difluorobenzyl)-1*H*-indazol-3-yl]-4-(piperazin-1-yl)-2-(tetrahydro-2*H*-pyran-4-ylamino)benzamide (22).* Eluant for column chromatography: DCM/EtOH/NH₃ 5 N in MeOH = 100/10/1. ¹H NMR (400.5 MHz, DMSO-*d*₆) δ ppm 1.30–1.41 (m, 2 H) 1.88–1.98 (m, 2 H) 2.80–2.87 (m, 4 H) 3.17–3.22 (m, 4 H) 3.45–3.54 (m, 2 H) 3.62–3.72 (m, 1 H) 3.78–3.84 (m, 2 H) 4.04 (s, 2 H) 6.11 (d, *J* = 2.2 Hz, 1 H) 6.22 (dd, *J* = 9.0, 2.2 Hz, 1 H) 6.94–7.04 (m, 3 H) 7.25 (dd, *J* = 8.6, 1.6 Hz, 1 H) 7.40 (d, *J* = 8.6 Hz, 1 H) 7.48 (s, 1 H) 7.79 (d, *J* = 9.0 Hz, 1 H) 8.28 (d, *J* = 7.7 Hz, 1 H) 10.06 (s, 1 H) 12.62 (s, 1 H). LCMS (ESI) *m/z* 547 ($M + H$)⁺. HRMS (ESI) calcd for $C_{30}H_{32}F_2N_6O_2 + H^+$ 547.2628, found 547.2628.

*1-[4-{[5-(3,5-Difluorobenzyl)-1*H*-indazol-3-yl]carbamoyl}-3-(tetrahydro-2*H*-pyran-4-ylamino)benzyl]piperidine (23).* Eluant for column chromatography: DCM/MeOH/NH₃ 5 N in MeOH = 100/5/1. ¹H NMR (400.5 MHz, DMSO-*d*₆) δ ppm 1.32–1.44 (m, 3 H) 1.67–1.87 (m, 5 H) 1.95–2.02 (m, 2 H) 2.82–2.93 (m, 2 H) 3.32 (br s, 2 H) 3.44–3.54 (m, 2 H) 3.63–3.74 (m, 1 H) 3.82–3.91 (m, 2 H) 4.06 (s, 2 H) 4.23 (d, *J* = 5.37 Hz, 2 H) 6.75–6.81 (m, 1 H) 6.94–7.06 (m, 2 H) 7.13 (s, 1 H) 7.29 (dd, *J* = 8.66, 1.46 Hz, 1 H) 7.45 (d, *J* = 8.54 Hz, 1 H) 7.50 (s, 1 H) 7.96 (d, *J* = 8.05 Hz, 1 H) 8.00 (br s, 1 H) 10.14 (br s, 1 H) 10.54 (s, 1 H) 12.77 (br s, 1 H). LCMS (ESI) *m/z* 560 ($M + H$)⁺. HRMS (ESI) calcd for $C_{32}H_{35}F_2N_5O_2 + H^+$ 560.2832, found 560.2831.

*N-[5-(3,5-Difluorobenzyl)-1*H*-indazol-3-yl]-4-(1-methylpiperidin-4-yl)oxy]-2-(tetrahydro-2*H*-pyran-4-ylamino)benzyl]piperidine (24).* Eluant for column chromatography: DCM/EtOH/NH₃ 5 N in MeOH = 100/10/1. ¹H NMR (400.5 MHz, DMSO-*d*₆) δ ppm 1.30–1.41 (m, 2 H) 1.62–1.75 (m, 2 H) 1.87–2.00 (m, 4 H) 2.20–2.87 (br s, 5 H) 2.69 (br s, 2 H) 3.44–3.53 (m, 2 H) 3.63 (m, 1 H) 3.78–3.85 (m, 2 H) 4.04 (s, 2 H) 4.50 (br s, 1 H) 6.23–6.28 (m, 2 H) 6.95–7.04 (m, 3 H) 7.26 (dd, *J* = 8.7, 1.6 Hz, 1 H) 7.42 (d, *J* = 8.6 Hz, 1 H) 7.49 (s, 1 H) 7.85–7.89 (m, 1 H) 8.21 (d, *J* = 7.7 Hz, 1 H) 10.24 (s, 1 H) 12.67 (s, 1 H). LCMS (ESI) *m/z* 576 ($M + H$)⁺. HRMS (ESI) calcd for $C_{32}H_{35}F_2N_5O_3 + H^+$ 576.2781, found 576.2773.

*N-[5-[1-(3,5-Difluoro-phenyl)-ethyl]-1*H*-indazol-3-yl]-4-(4-methyl-piperazin-1-yl)-2-(tetrahydro-pyran-4-ylamino)-benzamide (25).* Eluant for column chromatography: DCM/EtOH/NH₃ 5 N in MeOH = 100/5/2. ¹H NMR (400.5 MHz, DMSO-*d*₆) δ ppm 1.30–1.40 (m, 2 H) 1.60 (d, *J* = 7.2 Hz, 3 H) 1.89–1.98 (m, 2 H) 2.28 (br s, 3 H) 2.50 (overlapped by DMSO-*d*₆ signal, 4 H) 3.30 (overlapped by water signal, 4 H) 3.46–3.54 (m, 2 H) 3.64–3.74 (m, 1 H) 3.78–3.85 (m, 2 H) 4.31 (q, *J* = 7.2 Hz, 1 H) 6.15 (d, *J* = 2.0 Hz, 1 H) 6.25 (dd, *J* = 9.0, 2.0 Hz, 1 H) 6.95–7.03 (m, 3 H) 7.27 (dd, *J* = 8.7, 1.6 Hz, 1 H) 7.40 (d, *J* = 8.7 Hz, 1 H) 7.51 (s, 1 H) 7.80 (d, *J* = 9.0 Hz, 1 H) 8.31 (d, *J* = 7.7 Hz, 1 H) 10.08 (s, 1 H) 12.62 (s, 1 H). LCMS (ESI) *m/z* 576 ($M + H$)⁺. HRMS (ESI) calcd for $C_{32}H_{36}F_2N_5O_3 + H^+$ 576.2793.

*N-[5-Benzyl-1*H*-indazol-3-yl]-4-(4-methyl-piperazin-1-yl)-2-(tetrahydro-pyran-4-ylamino)-benzamide (28).* Eluant for column chromatography: DCM/EtOH/NH₃ 5 N in MeOH = 100/10/1. ¹H NMR (400.5 MHz, DMSO-*d*₆) δ ppm 1.30–1.41 (m, 2 H) 1.89–1.98 (m, 2 H) 2.23 (s, 3 H) 2.40–2.46 (m, 4 H) 3.23–3.30 (m, 4 H) 3.46–3.54 (m, 2 H) 3.63–3.73 (m, 1 H) 3.78–3.85 (m, 2 H) 4.01 (s, 2 H) 6.13 (d, *J* = 2.2 Hz, 1 H) 6.23 (dd, *J* = 9.0, 2.2 Hz, 1 H) 7.13–7.29 (m, 6 H) 7.37 (d, *J* = 8.9 Hz, 1 H) 7.43 (s, 1 H) 7.78 (d, *J* = 9.0 Hz, 1 H) 8.27 (d, *J* = 7.7 Hz, 1 H) 10.04 (s, 1 H) 12.58 (s, 1 H). LCMS (ESI) *m/z* 525 ($M + H$)⁺. HRMS (ESI) calcd for $C_{31}H_{36}N_6O_2 + H^+$ 525.2973, found 525.2983.

*N-[5-(2-Fluoro-benzyl)-1*H*-indazol-3-yl]-4-(4-methyl-piperazin-1-yl)-2-(tetrahydro-pyran-4-ylamino)-benzamide (29).* Eluant for

column chromatography: DCM/EtOH/NH₃ 5 N in MeOH = 100/10/1. ¹H NMR (400.5 MHz, DMSO-*d*₆) δ ppm 1.29–1.40 (m, 2 H) 1.89–1.98 (m, 2 H) 2.23 (s, 3 H) 2.40–2.48 (m, 4 H) 3.22–3.30 (m, 4 H) 3.45–3.53 (m, 2 H) 3.63–3.73 (m, 1 H) 3.77–3.85 (m, 2 H) 4.03 (s, 2 H) 6.14 (d, *J* = 2.2 Hz, 1 H) 6.24 (dd, *J* = 9.0, 2.2 Hz, 1 H) 6.95–7.02 (m, 1 H) 7.04–7.09 (m, 1 H) 7.10–7.12 (m, 1 H) 7.24 (dd, *J* = 8.6, 1.5 Hz, 1 H) 7.27–7.34 (m, 1 H) 7.40 (d, *J* = 8.9 Hz, 1 H) 7.46 (s, 1 H) 7.79 (d, *J* = 9.0 Hz, 1 H) 8.28 (d, *J* = 7.8 Hz, 1 H) 10.07 (s, 1 H) 12.61 (s, 1 H). LCMS (ESI) *m/z* 543 (M + H)⁺. HRMS (ESI) calcd for C₃₁H₃₅FN₆O₂ + H⁺ 543.2879, found 543.2864.

N-[5-(2,5-Difluoro-benzyl)-1*H*-indazol-3-yl]-4-(4-methyl-piperazin-1-yl)-2-(tetrahydro-pyran-4-ylamino)-benzamide (**30**). Eluant for column chromatography: DCM/EtOH/NH₃ 5 N in MeOH = 100/5/2. ¹H NMR (400.5 MHz, DMSO-*d*₆) δ ppm 1.28–1.41 (m, 2 H) 1.88–1.98 (m, 2 H) 2.26 (br s, 3 H) 2.42–2.48 (m, 4 H) 3.23–3.31 (m, 4 H) 3.44–3.55 (m, 2 H) 3.63–3.73 (m, 1 H) 3.78–3.85 (m, 2 H) 4.03 (s, 2 H) 6.13 (d, *J* = 2.2 Hz, 1 H) 6.24 (dd, *J* = 9.0, 2.2 Hz, 1 H) 7.03–7.11 (m, 1 H) 7.14–7.22 (m, 2 H) 7.24 (dd, *J* = 8.6, 1.0 Hz, 1 H) 7.40 (d, *J* = 8.6 Hz, 1 H) 7.45 (s, 1 H) 7.79 (d, *J* = 9.0 Hz, 1 H) 8.29 (d, *J* = 7.7 Hz, 1 H) 10.07 (s, 1 H) 12.62 (s, 1 H). LCMS (ESI) *m/z* 561 (M + H)⁺. HRMS (ESI) calcd for C₃₁H₃₄F₂N₆O₂ + H⁺ 561.2784, found 561.2790.

N-[5-(2-Methyl-5-fluoro-benzyl)-1*H*-indazol-3-yl]-4-(4-methyl-piperazin-1-yl)-2-(tetrahydro-pyran-4-ylamino)-benzamide (**31**). Eluant for column chromatography: DCM/EtOH/NH₃ 5 N in MeOH = 100/5/1. ¹H NMR (400.5 MHz, DMSO-*d*₆) δ ppm 1.28–1.40 (m, 2 H) 1.89–1.97 (m, 2 H) 2.21 (s, 3 H) 2.24 (br s, 3 H) 2.41–2.48 (m, 4 H) 3.23–3.29 (m, 4 H) 3.45–3.53 (m, 2 H) 3.63–3.73 (m, 1 H) 3.78–3.85 (m, 2 H) 4.02 (s, 2 H) 6.12 (d, *J* = 2.1 Hz, 1 H) 6.22 (dd, *J* = 9.0, 2.1 Hz, 1 H) 6.88–6.97 (m, 2 H) 7.14–7.20 (m, 2 H) 7.37 (s, 1 H) 7.40 (d, *J* = 8.6 Hz, 1 H) 7.78 (d, *J* = 9.0 Hz, 1 H) 8.30 (d, *J* = 7.8 Hz, 1 H) 10.06 (s, 1 H) 12.60 (s, 1 H). LCMS (ESI) *m/z* 557 (M + H)⁺. HRMS (ESI) calcd for C₃₂H₃₇FN₆O₂ + H⁺ 557.3035, found 557.3024.

2-Amino-N-[5-(3,5-difluoro-benzyl)-1*H*-indazol-3-yl]-4-(4-methyl-piperazin-1-yl)-benzamide (**4**). A mixture of *N*-[5-(3,5-difluorobenzyl)-1*H*-indazol-3-yl]-4-(4-methyl-piperazin-1-yl)-2-nitro-benzamide (**4**, 3.21 g, 6.33 mmol), cyclohexene (20 mL), dioxane (200 mL), and 10% Pd/C (0.8 g) was stirred at 100 °C for 2 h. The reaction mixture was filtered over a Celite pad washing thoroughly with THF and MeOH. After evaporation of the organic phase, purification of the crude by chromatography over silica gel (DCM/MeOH 95/5) gave 2.51 g of title compound (83% yield). ¹H NMR (400.5 MHz, DMSO-*d*₆) δ ppm 2.23 (s, 3 H) 2.40–2.47 (m, 4 H) 3.17–3.22 (m, 4 H) 4.04 (s, 2 H) 6.18 (d, *J* = 2.4 Hz, 1 H) 6.24 (dd, *J* = 9.0, 2.4 Hz, 1 H) 6.53 (br s, 2 H) 6.93–7.03 (m, 3 H) 7.22 (dd, *J* = 8.7, 1.6 Hz, 1 H) 7.39 (d, *J* = 8.7 Hz, 1 H) 7.52 (br s, 1 H) 7.72 (d, *J* = 9.0 Hz, 1 H) 10.01 (s, 1 H) 12.60 (s, 1 H). LCMS (ESI) *m/z* 477 (M + H)⁺. HRMS (ESI) calcd for C₂₆H₂₆F₂N₆O + H⁺ 477.2209, found 477.2207.

N-[5-(3,5-Difluorobenzyl)-1*H*-indazol-3-yl]-2-[*(2-hydroxyethyl)amino*-4-(4-methylpiperazin-1-yl)]benzamide (**11**). Crude 2-[*(2-[[tert-butyl(dimethyl)silyl]oxy]ethyl)amino*-*N*-[5-(3,5-difluorobenzyl)-1*H*-indazol-3-yl]-4-(4-methylpiperazin-1-yl)]benzamide (**10**, 0.2 mmol) was dissolved in dry THF (3 mL), and 1 M TBAF in THF (0.24 mL) was added at 0 °C. The resulting solution was stirred overnight at room temperature. Reaction was quenched with water and extracted with ethyl acetate. Collected organic phases were dried over Na₂SO₄, filtered, and evaporated to dryness. Residue was purified by column chromatography over silica gel (DCM/EtOH/NH₃ 5 N in MeOH = 85/15/1), affording 83 mg of title compound (80% yield). ¹H NMR (400.5 MHz, DMSO-*d*₆) δ ppm 2.32 (br s, 3 H) 2.54 (br s, 4 H) 3.19 (td, *J* = 5.6, 5.2 Hz, 2 H) 3.30 (m overlapped by water signal, 4 H) 3.58 (td, *J* = 5.5, 5.1 Hz, 2 H) 4.04 (s, 2 H) 4.74 (t, *J* = 5.1 Hz, 1 H) 6.08 (d, *J* = 2.1 Hz, 1 H) 6.24 (dd, *J* = 8.9, 2.1 Hz, 1 H) 6.94–7.04 (m, 3 H) 7.23 (dd, *J* = 8.6, 1.6 Hz, 1 H) 7.40 (d, *J* = 8.6 Hz, 1 H) 7.50 (s, 1 H) 7.77 (d, *J* = 8.9 Hz, 1 H) 8.21 (t, *J* = 5.2 Hz, 1 H) 10.05 (s, 1 H) 12.61 (s, 1 H). LCMS (ESI) *m/z* 521 (M + H)⁺. HRMS (ESI) calcd for C₂₈H₃₀F₂N₆O₂ + H⁺ 521.2471, found 521.2465.

N-[5-(3,5-Difluorobenzyl)-1*H*-indazol-3-yl]-2-[*(trans*-4-hydroxycyclohexyl)amino]-4-(4-methylpiperazin-1-yl)benzamide (**17**). Crude *trans*-4-{[2-[[5-(3,5-difluorobenzyl)-1*H*-indazol-3-yl]-carbamoyl]-5-(4-methylpiperazin-1-yl)phenyl]amino}cyclohexyl benzoate (**16**, 1.0 mmol) was dissolved in MeOH (100 mL) and water (10 mL) and treated at 60 °C with LiOH hydrate (125 mg, 3.0 mmol) for 4 h. MeOH was evaporated, and the resulting aqueous phase was extracted with ethyl acetate. Collected organic phases were dried over Na₂SO₄, filtered, and evaporated to dryness. Residue was purified by column chromatography over silica gel (DCM/EtOH/NH₃ 5 N in MeOH = 100/10/2), affording 233 mg of title compound (40% yield). ¹H NMR (400.5 MHz, DMSO-*d*₆) δ ppm 1.10–1.22 (m, 2 H) 1.28–1.42 (m, 2 H) 1.75–1.86 (m, 2 H) 1.94–2.03 (m, 2 H) 2.23 (s, 3 H) 2.41–2.46 (m, 4 H) 3.22–3.28 (m, 4 H) 3.34–3.42 (m, 1 H) 3.43–3.52 (m, 1 H) 4.03 (s, 2 H) 4.52 (d, *J* = 4.1 Hz, 1 H) 6.08 (d, *J* = 2.1 Hz, 1 H) 6.21 (dd, *J* = 9.0, 2.1 Hz, 1 H) 6.94–7.03 (m, 3 H) 7.24 (dd, *J* = 8.5, 1.6 Hz, 1 H) 7.40 (d, *J* = 8.5 Hz, 1 H) 7.47 (s, 1 H) 7.76 (d, *J* = 9.0 Hz, 1 H) 8.16 (d, *J* = 7.8 Hz, 1 H) 10.03 (s, 1 H) 12.61 (s, 1 H). LCMS (ESI) *m/z* 543 (M + H)⁺. HRMS (ESI) calcd for C₃₁H₃₅FN₆O₂ + H⁺ 543.2879, found 543.2864.

By employing the above-described procedure, the following compound was prepared.

N-[5-(3,5-Difluorobenzyl)-1*H*-indazol-3-yl]-2-[*(cis*-4-hydroxycyclohexyl)amino]-4-(4-methylpiperazin-1-yl)benzamide (**19**). Eluant for column chromatography: DCM/EtOH/NH₃ 5 N in MeOH = 100/10/2. ¹H NMR (400.5 MHz, DMSO-*d*₆) δ ppm 1.41–1.70 (m, 8 H) 2.23 (s, 3 H) 2.40–2.47 (m, 4 H) 3.20–3.28 (m, 4 H) 3.50–3.64 (m, 2 H) 4.04 (s, 2 H) 4.42 (d, *J* = 3.8 Hz, 1 H) 6.08 (d, *J* = 1.9 Hz, 1 H) 6.21 (dd, *J* = 8.9, 2.2 Hz, 1 H) 6.94–7.04 (m, 3 H) 7.24 (dd, *J* = 8.6, 1.6 Hz, 1 H) 7.40 (d, *J* = 8.5 Hz, 1 H) 7.50 (s, 1 H) 7.78 (d, *J* = 9.0 Hz, 1 H) 8.38 (d, *J* = 7.7 Hz, 1 H) 10.03 (s, 1 H) 12.62 (s, 1 H). LCMS (ESI) *m/z* 575 (M + H)⁺. HRMS (ESI) calcd for C₃₂H₃₆F₂N₆O₂ + H⁺ 575.2941, found 575.2943.

(S)- or (R)-*N*-[5-(1-(3,5-Difluorophenyl)ethyl)-1*H*-indazol-3-yl]-4-(4-methylpiperazin-1-yl)-2-(tetrahydro-2*H*-pyran-4-ylamino)-benzamide (**26**) and (**27**). Single enantiomers (**26** and **27**) have been obtained from racemate **25** by preparative chiral-HPLC by using Daicel Chiralpak AD 250 mm × 20 mm 10 μm as column system and *n*-hexane/2-propanol 40:60 as eluant (flow rate 6 mL/min): first peak eluted = **26**, second peak eluted = **27**.

26: ¹H NMR (400.5 MHz, DMSO-*d*₆) δ ppm 1.30–1.40 (m, 2 H) 1.60 (d, *J* = 7.2 Hz, 3 H) 1.89–1.98 (m, 2 H) 2.27 (br s, 3 H) 2.50 (overlapped by DMSO-*d*₆ signal, 4 H) 3.30 (overlapped by water signal, 4 H) 3.46–3.54 (m, 2 H) 3.64–3.74 (m, 1 H) 3.78–3.85 (m, 2 H) 4.31 (q, *J* = 7.2 Hz, 1 H) 6.15 (d, *J* = 2.0 Hz, 1 H) 6.25 (dd, *J* = 9.0, 2.0 Hz, 1 H) 6.95–7.03 (m, 3 H) 7.27 (dd, *J* = 8.7, 1.6 Hz, 1 H) 7.40 (d, *J* = 8.7 Hz, 1 H) 7.51 (s, 1 H) 7.80 (d, *J* = 9.0 Hz, 1 H) 8.31 (d, *J* = 7.7 Hz, 1 H) 10.08 (s, 1 H) 12.62 (s, 1 H). LCMS (ESI) *m/z* 575 (M + H)⁺. HRMS (ESI) calcd for C₃₂H₃₆F₂N₆O₂ + H⁺ 575.2941, found 575.2944.

27: ¹H NMR (400.5 MHz, DMSO-*d*₆) δ ppm 1.30–1.40 (m, 2 H) 1.60 (d, *J* = 7.2 Hz, 3 H) 1.89–1.98 (m, 2 H) 2.25 (s, 3 H) 2.43–2.50 (m, 4 H) 3.24–3.31 (m, 4 H) 3.46–3.54 (m, 2 H) 3.64–3.74 (m, 1 H) 3.78–3.85 (m, 2 H) 4.31 (q, *J* = 7.2 Hz, 1 H) 6.15 (d, *J* = 2.0 Hz, 1 H) 6.25 (dd, *J* = 9.0, 2.0 Hz, 1 H) 6.95–7.03 (m, 3 H) 7.27 (dd, *J* = 8.7, 1.6 Hz, 1 H) 7.40 (d, *J* = 8.7 Hz, 1 H) 7.51 (s, 1 H) 7.80 (d, *J* = 9.0 Hz, 1 H) 8.31 (d, *J* = 7.7 Hz, 1 H) 10.08 (s, 1 H) 12.62 (s, 1 H). LCMS (ESI) *m/z* 575 (M + H)⁺. HRMS (ESI) calcd for C₃₂H₃₆F₂N₆O₂ + H⁺ 575.2941, found 575.2943.

2. High-Throughput Screening. More than 50000 compounds of our Corporate Compound Collection were tested at 10 μM using KinaseGlo assay format (Promega). Recombinant ALK protein was tested at low ATP concentration (1/8 fold appKm ATP) and at 2 μM MBP (Myelin Basic Protein). After an incubation time at room temperature for 90 min, KinaseGlo reagent was added and the luminescent signal was read using ViewLux Reader (PerkinElmer).

3. Kinase Assays. The potency of entrectinib toward ALK and its selectivity toward additional kinases was tested using a highly diverse panel of tyrosine and serine-threonine kinases called kinase selectivity screening (KSS), based on measurement of phosphorylated substrate

after capture of non reacted γ -33-ATP with a strong anion exchanger (Dowex 1-X8 resin, formate form), as previously described.³⁷ For each enzyme, the absolute K_m values for ATP and the specific substrate were initially determined, and each assay is run at optimized ATP (2 K_m) and substrate (5 K_m) concentrations. Because under these conditions $IC_{50} = 3\beta K_i$ according to the Cheng–Prusoff relation for competitive inhibitors, these conditions enable direct comparison of IC_{50} values among the different enzymes of the KSS panel for the evaluation of inhibitor biochemical selectivity. All assays were performed in house, with the exception of TRKB and TRKC, for which IC_{50} s were extrapolated from percentage inhibition values obtained at 10 and 100 nM of inhibitor in duplicate employing the SelectScreen Kinase Profiling Services from Life Technologies using the equation: $IC_{50\text{extrap}} = ([I] \times 100/\% \text{ inhibition}) - [I]$, with the assumption that Hill slope = 1.

K_i determination: Enzymatic activity at different ATP and Substrate concentrations was evaluated in the presence of different concentrations of entrectinib. The experiment has been done at initial velocity, substrates consumption <10%, in 96-well plate. The data obtained were analyzed using different models and a statistical approach was used in order to choose the most probable mechanism of inhibition to calculate the K_i .

4. Crystallization and Structure Determination. Crystals of the two ALK–inhibitor complexes here presented were obtained following the procedures previously described.³³ X-ray diffraction data from the ALK–2 crystal were collected in house using a Rigaku Micromax-007 HF X-ray generator and Mar345 image plate detector (Marresearch), while data from the ALK–17 crystal were collected at ESRF in Grenoble, on beamline ID23-1. Indexing, integration, and scaling were performed using MOSFLM and SCALA.³⁸ Both ALK-KD structures were determined by molecular replacement using Phaser.³⁹ The search model was the structure of the ALK-KD-PHA-E429 complex (PDB ID 2XBA). Model building was done using Coot,⁴⁰ and refinement was done with RefMac.⁴¹ Crystallographic data are listed in Table S1 (see Supporting Information). Structural images have been generated with PyMol v1.3.⁴²

5. High-Throughput Solubility. Solubility at pH 7 was performed as previously described.⁴³

6. Cell Permeability. Caco-2 permeability assay was performed as previously described.^{44,45}

7. Intrinsic Clearance Determination in HLM (Human Liver Microsomes). Intrinsic clearance in human liver microsomes was determined as previously described.⁴⁵

8. Intrinsic Clearance Determination in Rat Hepatocytes. Intrinsic clearance in human liver microsomes was determined as previously described.⁴⁵

9. In Vivo Pharmacokinetics. Pharmacokinetic properties were investigated in mouse (nu/nu), rat (Han Wistar), and beagle dogs after single intravenous and oral administration. Plasma levels of the compounds were determined by protein precipitation in a 96-well plate format followed by LC-MS/MS analysis. The limits of quantification were 5–20000 ng/mL. Pharmacokinetic data analysis was carried out using a noncompartmental approach (linear trapezoidal rule) with the aid of WinNonlin software (v3.1; Pharsight, Inc.).

For the analysis of brain levels, entrectinib was orally administered for 14 consecutive days and 6 h after last administration mice were eutanized, plasma and brain were collected and analyzed as previously reported.⁴⁶

10. Cell Culture. Human cancer cell lines were obtained from ATCC, from ECACC, from Interlab Cell Line Collection (ICLC) and from NCI. Cells were maintained in the media recommended by the suppliers, in a humidified 37 °C incubator with 5% CO₂. The identity of all cell lines used in this study was verified using DNA fingerprinting technology (AmpFlSTR Identifier Plus PCR amplification kit, Applied Biosystems).

11. Generation of Oncogene-Driven Ba/F3 Cells. Ba/F3_EML4/ALK were generated as previously reported.³⁴ To generate tyrosine kinases fused to the human ETV6/TEL partner, a plasmid based on a pcDNA3.1 DEST backbone was constructed that allowed

rapid in-frame cloning of the kinase domains downstream of a Tel cassette using a Gateway system. The constructs obtained were the result of the 336 NH2-residues of TEL fused to the amino acids residues of ROS1 (1891–2347), TRKA (440–796), TRKB (455–822), and TRKC (454–825). The pcDNA expression vectors were introduced into the murine IL-3 dependent pro-B Ba/F3 cells (DSMZ) by electroporation (Amaxa Nucleofector II device) using the “Amaxa Cell Line Nucleofector Kit V” (VCA-1003), according to manufacturer protocol. Stable strains of IL-3 independent Ba/F3 cells were established by post-transfection selection of cells for 2 weeks with 800 µg/mL G418 (Enzo Life Sciences) and subsequent growth in medium lacking IL-3.

12. Analysis of Cell Proliferation. To evaluate the antiproliferative activity of test compounds cells were seeded into 384-well plates in appropriate complete medium. Twenty-four hours after seeding, cells were treated with serial dilutions of test compounds in medium at a final concentration of 0.1% DMSO and incubated for additional 72 h. At the end of treatment, cell viability was assessed using the CellTiter-Glo luciferase-based ATP detection assay (Promega) following manufacturer's instructions. CellTiter-Glo is a homogeneous assay method based on the quantification of ATP present, an indicator of the number of metabolically active cells. Growth inhibitory activity was evaluated comparing data for treated versus control samples, using Accelrys Assay Explorer software. IC_{50} values were calculated using sigmoidal interpolation curve fitting.

13. Western Blot Analysis. Cellular mechanism of action of compound 2 was investigated by treating cells with different concentrations of the compound for 2 h at 37 °C. Treated cells were washed twice with ice-cold phosphate buffered saline (PBS) and lysed in a buffer containing 100 mM Tris-HCl pH 7.4, 2% SDS, 1 mM DTT, 1 mM sodium orthovanadate, and 1 mM EDTA. Cell extracts were immediately boiled for 10 min, briefly sonicated, clarified by centrifugation, and analyzed for protein content (BCA Protein Assay, Pierce). Protein extracts were separated by SDS-PAGE and analyzed by immunoblotting following standard procedures. Staining was performed with the following antibodies: Phospho-TRKA-Tyr490 and TRKA from Calbiochem, Phospho-ALK-Tyr1604, ALK, Phospho-PLC γ 1-Tyr783, PLC γ 1, Phospho-STAT3-Tyr705, Phospho-AKT-Ser473, AKT, Phospho-MAPK-Thr202/Tyr204, and MAPK from Cell Signaling, STAT3 from BD Biosciences.

14. Efficacy Studies and ex Vivo Target Modulation Analysis. All procedures adopted for housing and handling of animals were in strict compliance with Italian and European guidelines for Laboratory Animal Welfare. A total of 10^7 NCI-H2228 nonsmall cell lung cancer cells were transplanted subcutaneously in athymic nu/nu mice (Harlan). For the ALCL model, a total of 10^7 Karpas-299 cells were transplanted subcutaneously in SCID mice (Harlan) previously pretreated with total body irradiation at 2 Gy. Mice bearing a minimal tumor mass (150–250 mm³) were randomized into vehicle and treated groups. Oral treatments started the day after randomization, with different doses as described. Tumor dimensions were measured regularly using Vernier calipers, and tumor volume was calculated according to the following formula: length (mm) × width² (mm)/2. The percentage of tumor inhibition (%TI) was calculated as follows: % TI = 100 – (mean tumor volume of treated group/mean tumor volume of control group) × 100. Toxicity was evaluated on the basis of body weight reduction. At the end of the experiment, mice were sacrificed and gross autopsy findings were reported. Tumor-free animals at 90 days after tumor implant were considered cured. For ex vivo target modulation analysis, animals bearing established xenograft tumors were treated with a single orally administered dose and sacrificed at 12 and 18 h following treatment. Xenograft tumor samples were snap frozen in liquid nitrogen immediately after excision and stored at –80 °C until analyzed. The frozen samples were homogenized using an Ultra Turrax T25 potter (Janke and Kunkel) at a 5:1 ratio (v/w) in a lysis buffer containing 100 mM Tris-HCl pH 7.4, 2% SDS, 1 mM EDTA, 1 mM sodium orthovanadate, and 1 mM DTT and immediately boiled. Tumor lysates were briefly sonicated, clarified by centrifugation, assayed for protein content, and used for SDS-PAGE and Western blotting analysis.

■ ASSOCIATED CONTENT

● Supporting Information

The Supporting Information is available free of charge on the ACS Publications website at DOI: [10.1021/acs.jmedchem.6b00064](https://doi.org/10.1021/acs.jmedchem.6b00064).

Data collection, refinement statistics, and crystallographic structures for the two ALK inhibitors **2** and **17** in complex with the ALK protein; biochemical potency, lipophilicity, and lipophilic ligand efficiency of the ALK inhibitors ([PDF](#))

Molecular formula strings ([CSV](#))

Accession Codes

Atomic coordinates for the crystal structures of ALK with compounds **2** and **17** can be accessed using PDB codes SFTO and SFTQ, respectively.

■ AUTHOR INFORMATION

Corresponding Author

*Phone: +39-0331-581928. Fax: +39-0331-581347. E-mail: maria.menichincheri@nervianoms.com.

Present Addresses

[§]For R.B.: Tecan Italia S.r.l., Via Brescia 39, 20063 Cernusco sul Naviglio, Milan, Italy.

[¶]For C.F.: Chiesi Farmaceutici S.p.A., Nuovo Centro Ricerche, Largo Belloli 11/a, 43122 Parma, Italy.

Notes

The authors declare no competing financial interest.

■ ACKNOWLEDGMENTS

We are grateful to the personnel of the Biochemical and Cellular Screening Department, particularly Antonella Leone and Dario Ballinari. Thanks are also due to Elena Casale for helpful discussion and support, to Tiziano Bandiera for his valuable contribution to the project, and to Luca Mologni (University of Milano-Bicocca, Monza, Italy) for providing us the Ba/F3 cell lines transfected with EML4-ALK wild type and mutants.

■ ABBREVIATIONS USED

ABL, Abelson tyrosine kinase gene; ADME, absorption, distribution, metabolism, and excretion; ALCL, anaplastic large cell lymphoma; ALK, anaplastic lymphoma kinase; ATP, adenosine triphosphate; BCR, breakpoint cluster region; *n*-BuOH, *n*-butanol; CML, chronic myelogenous leukemia; CRC, colorectal cancer; DCM, dichloromethane; DIPEA, *N,N*-diisopropylethylamine; DMF, *N,N*-dimethylformamide; DMSO, dimethyl sulfoxide; EGFR, epidermal growth factor receptor; EML4, echinoderm microtubule-associated protein-like-4; EtOH, ethanol; FDA, Food and Drug Administration; FIG, fused in glioblastoma gene; HPLC, high-performance liquid chromatography; HTS, high-throughput screening; IMT, inflammatory myofibroblastic tumors; IGFR1, insulin-like growth factor1 receptor; IL-3, interleukin-3; IR, insulin receptor; LiHMDS, bis(trimethylsilyl)-lithiumamid; MeOH, methanol; NGF, nerve growth factor; NPM, nucleophosmin; NSCLC, nonsmall cell lung cancer; NTRK1, neurotrophic tyrosine kinase receptor1; PAMPA, parallel artificial membrane permeability; RTK, receptor tyrosine kinase; ROS1, c-ras oncogene 1; SAR, structure–activity relationship; SCID, severe combined immune deficiency; TBAF, tetra-*n*-butylammonium

fluoride; TEA, triethylamine; THF, tetrahydrofuran; TPM3, tropomyosin 3; TRK, tropomyosin receptor kinase

■ REFERENCES

- (1) Deininger, M.; Buchdunger, E.; Druker, B. J. The development of imatinib as a therapeutic agent for chronic myeloid leukemia. *Blood* **2005**, *105*, 2640–2653.
- (2) Tsao, M. S.; Sakurada, A.; Cutz, J. C.; Zhu, C. Q.; Kamel-Reid, S.; Squire, J.; Lorimer, I.; Zhang, T.; Liu, N.; Daneshmand, M.; Marrano, P.; da Cunha Santos, G.; Lagarde, A.; Richardson, F.; Seymour, L.; Whitehead, M.; Ding, K.; Pater, J.; Shepherd, F. A. Erlotinib in lung cancer - molecular and clinical predictors of outcome. *N. Engl. J. Med.* **2005**, *353*, 133–144.
- (3) Shaw, A. T.; Engelman, J. A. ALK in lung cancer: past, present, and future. *J. Clin. Oncol.* **2013**, *31*, 1105–1111.
- (4) Mossé, Y. P.; Wood, A.; Maris, J. M. Inhibition of ALK signalling for cancer therapy. *Clin. Cancer Res.* **2009**, *15*, 5609–5614.
- (5) Morris, S. W.; Kirstein, M. N.; Valentine, M. B.; Dittmer, K. G.; Shapiro, D. N.; Saltman, D. L.; Look, A. T. Fusion of a kinase gene ALK, to a nucleolar protein gene, NPM, in non-Hodgkin's. *Science* **1994**, *263*, 1281–1284.
- (6) Griffin, C. A.; Hawkins, A. L.; Dvorak, C.; Henkle, C.; Ellingham, T.; Perlman, E. J. Recurrent involvement of 2p23 in inflammatory myofibroblastic tumours. *Cancer Res.* **1999**, *59*, 2776–2780.
- (7) Soda, M.; Choi, Y. L.; Enomoto, M.; Takada, S.; Yamashita, Y.; Ishikawa, S.; Fujiwara, S.-I.; Watanabe, H.; Kurashina, K.; Hatanaka, H.; Bando, M.; Ohno, S.; Ishikawa, Y.; Aburatani, H.; Niki, T.; Sohara, Y.; Sugiyama, Y.; Mano, H. Identification of the transforming EML4–ALK fusion gene in non-small-cell lung cancer. *Nature* **2007**, *448*, 561–566.
- (8) Rikova, K.; Guo, A.; Zeng, O.; Possemato, A.; Yu, J.; Haack, H.; Nardone, J.; Lee, K.; Reeves, C.; Li, Y.; Hu, Y.; Tan, Z.; Stokes, M.; Sullivan, L.; Mitchell, J.; Wetzel, R.; MacNeill, J.; Ren, J. M.; Yuan, J.; Bakalarski, C. E.; Villen, J.; Kornhauser, J. M.; Smith, B.; Li, D.; Zhou, X.; Gygi, S. P.; Gu, T.-L.; Polakiewicz, R. D.; Rush, J.; Comb, M. J. Global survey of phosphotyrosine signalling identifies oncogenic kinases in lung cancer. *Cell* **2007**, *131*, 1190–1203.
- (9) Mossé, Y. P.; Laudenslager, M.; Longo, L.; Cole, K. A.; Wood, A.; Attiyeh, E. F.; Laquaglia, M. J.; Sennett, R.; Lynch, J. E.; Perri, P.; Laureys, G.; Speleman, F.; Kim, C.; Hou, C.; Hakonarson, H.; Torkamani, A.; Schork, N. J.; Brodeur, G. M.; Tonini, G. P.; Rappaport, E.; Devoto, M.; Maris, J. M. Identification of ALK as a major familial neuroblastoma predisposition gene. *Nature* **2008**, *455*, 930–935.
- (10) Janoueix-Lerosey, I.; Lequin, D.; Brugières, L.; Ribeiro, A.; de Pontual, L.; Combaret, V.; Raynal, V.; Puisieux, A.; Schleiermacher, G.; Pierron, G.; Valteau-Couanet, D.; Frebourg, T.; Michon, J.; Lyonnet, S.; Amiel, J.; Delattre, O. Somatic and germline activating mutations of the ALK kinase receptor in neuroblastoma. *Nature* **2008**, *455*, 967–970.
- (11) Chen, Y.; Takita, J.; Choi, Y. L.; Kato, M.; Ohira, M.; Sanada, M.; Wang, L.; Soda, M.; Kikuchi, A.; Igarashi, T.; Nakagawara, A.; Hayashi, Y.; Mano, H.; Ogawa, S. Oncogenic mutations of ALK kinase in neuroblastoma. *Nature* **2008**, *455*, 971–974.
- (12) George, R. E.; Sanda, T.; Hanna, M.; Fröhling, S.; Luther, W., II; Zhang, J.; Ahn, Y.; Zhou, W.; London, W. B.; McGrady, P.; Xue, L.; Zozulya, S.; Gregor, V. E.; Webb, T. R.; Gray, N. S.; Gilliland, D. G.; Diller, L.; Greulich, H.; Morris, S. W.; Meyerson, M.; Look, A. T. Activating mutations in ALK provide a therapeutic target in neuroblastoma. *Nature* **2008**, *455*, 975–978.
- (13) (a) Christensen, J. G.; Zou, H. Y.; Arango, M. E.; Li, Q.; Lee, J. H.; McDonnell, S. R.; Yamazaki, S.; Alton, G. R.; Mroczkowski, B.; Los, G. Cytoreductive antitumor activity of PF-2341066, a novel inhibitor of anaplastic lymphoma kinase and c-Met, in experimental models of anaplastic large-cell lymphoma. *Mol. Cancer Ther.* **2007**, *6*, 3314–3322. (b) Cui, J. J.; Tran-Dube, M.; Shen, H.; Nambu, M.; Kung, P. P.; Pairish, M.; Jia, L.; Meng, J.; Funk, L.; Botrous, I.; McGigue, M.; Grodsky, N.; Ryan, K.; Padrique, E.; Alton, G.; Timofeevski, S.; Yamazaki, S.; Li, Q.; Zou, H.; Christensen, J.;

- Mroczkowski, B.; Bender, S.; Kania, R. S.; Edwards, M. P. Structure based drug design of crizotinib (PF-02341066), a potent and selective dual inhibitor of mesenchymal–epithelial transition factor (c-MET) kinase and anaplastic lymphoma kinase (ALK). *J. Med. Chem.* **2011**, *54* (18), 6342–6363. (c) Cui, J. J.; McTigue, M.; Kania, R.; Edwards, M. Case history: XalkoriTM (Crizotinib), a potent and selective dual inhibitor of mesenchymal epithelial transition (MET) and anaplastic lymphoma kinase (ALK) for cancer treatment. *Annu. Rep. Med. Chem.* **2013**, *48*, 421–434.
- (14) Marsilje, T. H.; Pei, W.; Chen, B.; Lu, W.; Uno, T.; Jin, Y.; Jiang, T.; Kim, S.; Li, N.; Warmuth, M.; Sarkisova, Y.; Sun, F.; Steffy, A.; Pferdekamper, A. C.; Li, A. G.; Joseph, S. B.; Kim, Y.; Liu, B.; Tuntland, T.; Cui, X.; Gray, N. S.; Steensma, R.; Wan, Y.; Jiang, J.; Chopiuk, G.; Li, J.; Gordon, W. P.; Richmond, W.; Johnson, K.; Chang, J.; Groessl, T.; He, Y.-Q.; Phimister, A.; Aycinena, A.; Lee, C. C.; Bursulaya, B.; Karanewsky, D. S.; Seidel, H. M.; Harris, J. L.; Michellys, P.-Y. Synthesis, structure–activity relationships, and in vivo efficacy of the novel potent and selective anaplastic lymphoma kinase (ALK) inhibitor 5-chloro-N2-(2-isopropoxy-5-methyl-4-(piperidin-4-yl)phenyl)-N4-(2-(isopropylsulfonyl)-phenyl)pyrimidine-2,4-diamine (LDK378) currently in phase 1 and phase 2 clinical trials. *J. Med. Chem.* **2013**, *56*, S675–S690.
- (15) (a) Sakamoto, H.; Tsukaguchi, T.; Hiroshima, S.; Kodama, T.; Kobayashi, T.; Fukami, T. A.; Oikawa, N.; Tsukuda, T.; Ishii, N.; Aoki, Y. CH5424802, a selective ALK inhibitor capable of blocking the resistantgatekeeper mutant. *Cancer Cell* **2011**, *19*, 679–690. (b) Kinoshita, K.; Kobayashi, T.; Asoh, K.; Furuichi, N.; Ito, T.; Kawada, H.; Hara, S.; Ohwada, J.; Hattori, K.; Miyagi, T.; Hong, W.-S.; Park, M.-J.; Takanashi, K.; Tsukaguchi, T.; Sakamoto, H.; Tsukuda, T.; Oikawa, N. 9-Substituted 6,6-dimethyl-11-oxo-6,11-dihydro-5H-benzo[b]carbazoles as highly selective and potent anaplastic lymphoma kinase inhibitors. *J. Med. Chem.* **2011**, *54*, 6286–6294.
- (16) Katayama, R.; Khan, T. M.; Benes, C.; Lifshits, E.; Ebi, H.; Rivera, V. M.; Shakespeare, W. C.; Iafrate, A. J.; Engelman, J. A.; Shaw, A. T. Therapeutic strategies to overcome crizotinib resistance in non-small cell lung cancers harboring the fusion oncogene EML4-ALK. *Proc. Natl. Acad. Sci. U. S. A.* **2011**, *108* (18), 7535–7540.
- (17) Gainor, J. F.; Ou, S. H.; Logan, J.; Borges, L. F.; Shaw, A. T. The central nervous system as a sanctuary site in ALK-positive non-small-cell lung cancer. *J. Thorac. Oncol.* **2013**, *8*, 1570–1573.
- (18) Sasaki, T.; Okuda, K.; Zheng, W.; Butrynski, J.; Capelletti, M.; Wang, L.; Gray, N. S.; Wilner, K.; Christensen, J. G.; Demetri, G.; Shapiro, G. I.; Rodig, S. J.; Eck, M. J.; Jänne, P. A. The neuroblastoma-associated F1174L ALK mutation causes resistance to an ALK kinase inhibitor in ALK-translocated cancers. *Cancer Res.* **2010**, *70*, 10038–10043.
- (19) Choi, Y. L.; Soda, M.; Yamashita, Y.; Ueno, T.; Takashima, J.; Nakajima, T.; Yatabe, Y.; Takeuchi, K.; Hamada, T.; Haruta, H.; Ishikawa, Y.; Kimura, H.; Mitsudomi, T.; Tanio, Y.; Mano, H. ALK Lung Cancer Study Group. EML4-ALK mutations in lung cancer that confer resistance to ALK inhibitors. *N. Engl. J. Med.* **2010**, *363*, 1734–1739.
- (20) Katayama, R.; Shaw, A. T.; Khan, T. M.; Mino-Kenudson, M.; Solomon, B. J.; Halmos, B.; Jessop, N. A.; Wain, J. C.; Yeo, A. T.; Benes, C.; Drew, L.; Saeh, J. C.; Crosby, K.; Sequist, L. V.; Iafrate, A. J.; Engelman, J. A. Mechanisms of acquired crizotinib resistance in ALK-rearranged lung cancers. *Sci. Transl. Med.* **2012**, *4*, 120ra17.
- (21) Bergethon, K.; Shaw, T.; Ou, S. H. I.; Katayama, R.; Lovly, C. M.; McDonald, N. T.; Masson, P. P.; Siwak-Tapp, C.; Gonzalez, A.; Fang, R.; Mark, E. J.; Batten, J. M.; Chen, H.; Wilner, K. D.; Kwak, E. L.; Clark, J. W.; Carbone, D. P.; Ji, H.; Engelman, J. A.; Mino-Kenudson, M.; Pao, W.; Iafrate, A. J. ROS1 rearrangements define a unique molecular class of lung cancers. *J. Clin. Oncol.* **2012**, *30*, 863–870.
- (22) Greco, A.; Miranda, C.; Pierotti, M. A. Rearrangements of NTRK1 gene in papillary thyroid carcinoma. *Mol. Cell. Endocrinol.* **2010**, *321*, 44–49.
- (23) Vaishnavi, A.; Capelletti, M.; Le, A. T.; Kako, S.; Butaney, M.; Ercan, D.; Mahale, S.; Davies, K. D.; Aisner, D. L.; Pilling, A. B.; Berge, E. M.; Kim, J.; Sasaki, H.; Park, S. I.; Kryukov, G.; Garraway, L. A.; Hammerman, P. S.; Haas, J.; Andrews, S. W.; Lipson, D.; Stephens, P. J.; Miller, V. A.; Varella-Garcia, M.; Jänne, P. A.; Doebele, R. C. Oncogenic and drug-sensitive NTRK1 rearrangements in lung cancer. *Nat. Med.* **2013**, *19*, 1469–1472.
- (24) Ardini, E.; Bosotti, R.; Borgia, A. L.; De Ponti, C.; Somaschini, A.; Cammarota, R.; Amboldi, N.; Raddrizzani, L.; Milani, A.; Magnaghi, P.; Ballinari, D.; Casero, D.; Gasparri, F.; Banfi, P.; Avanzi, N.; Saccardo, M. B.; Alzani, R.; Bandiera, T.; Felder, E.; Donati, D.; Pesenti, E.; Sartore-Bianchi, A.; Gambacorta, M.; Pierotti, M. A.; Siena, S.; Veronese, S.; Galvani, A.; Isacchi, A. The TPM3-NTRK1 rearrangement is a recurring event in colorectal carcinoma and is associated with tumor sensitivity to TRKA kinase inhibition. *Mol. Oncol.* **2014**, *8*, 1495–1507.
- (25) Wiesner, T.; He, J.; Yelensky, R.; Esteve-Puig, R.; Botton, T.; Yeh, I.; Lipson, D.; Otto, G.; Brennan, K.; Murali, R.; Garrido, M.; Miller, V. A.; Ross, J. S.; Berger, M. F.; Sparatta, A.; Palmedo, G.; Cerroni, L.; Busam, K. J.; Kutzner, H.; Cronin, M. T.; Stephens, P. J.; Bastian, B. C. Kinase fusions are frequent in Spitz tumours and spitzoid melanoma. *Nat. Commun.* **2014**, *5*, 3116.
- (26) Ross, J. S.; Wang, K.; Gay, L.; Al-Rohil, R.; Rand, J. V.; Jones, D. M.; Lee, H. J.; Sheehan, C. E.; Otto, G. A.; Palmer, G.; Yelensky, R.; Lipson, D.; Morosini, D.; Hawryluk, M.; Catenacci, D. V.; Miller, V. A.; Churi, C.; Ali, S.; Stephens, P. J. New routes to targeted therapy of intrahepatic cholangiocarcinomas revealed by next-generation sequencing. *Oncologist* **2014**, *19*, 235–242.
- (27) Kim, J.; Lee, Y.; Cho, H. J.; Lee, Y. E.; An, J.; Cho, G. H.; Ko, Y. H.; Joo, K. M.; Nam, D. H. NTRK1 fusion in glioblastoma multiforme. *PLoS One* **2014**, *9*, e91940.
- (28) Wu, G.; Diaz, A. K.; Paugh, B. S.; Rankin, S. L.; Ju, B.; Li, Y.; Zhu, X.; Qu, C.; Chen, X.; Zhang, J.; Easton, J.; Edmonson, M.; Ma, X.; Lu, C.; Nagahawatte, P.; Hedlund, E.; Rusch, M.; Pounds, S.; Lin, T.; Onar-Thomas, A.; Huether, R.; Kriwacki, R.; Parker, M.; Gupta, P.; Becksfort, J.; Wei, L.; Mulder, H. L.; Boggs, K.; Vadodaria, B.; Yergeau, D.; Russell, J. C.; Ochoa, K.; Fulton, R. S.; Fulton, L. L.; Jones, C.; Boop, F. A.; Broniscer, A.; Wetmore, C.; Gajjar, A.; Ding, L.; Mardis, E. R.; Wilson, R. K.; Taylor, M. R.; Downing, J. R.; Ellison, D. W.; Zhang, J.; Baker, S. J. The genomic landscape of diffuse intrinsic pontine glioma and pediatric non-brainstem high-grade glioma. *Nat. Genet.* **2014**, *46*, 444–450.
- (29) Amatu, A.; Somaschini, A.; Cerea, G.; Bosotti, R.; Valtorta, E.; Buonandi, P.; Marrapese, G.; Veronese, S.; Luo, D.; Hornby, Z.; Multani, P.; Murphy, D.; Shoemaker, R.; Lauricella, C.; Giannetta, L.; Maiolani, M.; Vanzulli, A.; Ardini, E.; Galvani, A.; Isacchi, A.; Sartore-Bianchi, A.; Siena, S. Novel CAD-ALK gene rearrangement is druggable by entrectinib in colorectal cancer. *Br. J. Cancer* **2015**, *113*, 1730–1734.
- (30) Sartore-Bianchi, A.; Ardini, E.; Bosotti, R.; Amatu, A.; Valtorta, E.; Somaschini, A.; Raddrizzani, L.; Palmeri, L.; Banfi, P.; Bonazzina, E.; Misale, S.; Marrapese, G.; Leone, A.; Alzani, R.; Luo, D.; Hornby, Z.; Lim, J.; Veronese, S.; Vanzulli, A.; Bardelli, A.; Martignoni, M.; Davite, C.; Galvani, A.; Isacchi, A.; Siena, S. Sensitivity to entrectinib associated with a novel LMNA-NTRK1 gene fusion in metastatic colorectal cancer. *J. Natl. Cancer Inst.* **2016**, *108*, djv306.
- (31) Orsini, P.; Menichincheri, M.; Vanotti, E.; Panzeri, A. Highly efficient synthesis of 5-benzyl-3-aminoindazoles. *Tetrahedron Lett.* **2009**, *50*, 3098–3100.
- (32) Lombardi Borgia, A.; Menichincheri, M.; Orsini, P.; Panzeri, A.; Perrone, E.; Vanotti, E.; Nesi, M.; Marchionni, C. Substituted indazole derivatives active as kinase inhibitors. WO2009/013126 A1, 2009.
- (33) Bossi, R. T.; Saccardo, M. B.; Ardini, E.; Menichincheri, M.; Rusconi, L.; Magnaghi, P.; Orsini, P.; Avanzi, N.; Borgia, A. L.; Nesi, M.; Bandiera, T.; Fogliatto, G.; Bertrand, J. A. Crystal structure of anaplastic lymphoma kinase in complex with ATP competitive inhibitors. *Biochemistry* **2010**, *49*, 6813–6825.
- (34) Fontana, D.; Ceccon, M.; Gambacorti-Passernini, C.; Mologni, L. Activity of second-generation ALK inhibitors against crizotinib-resistant mutants in an NPM-ALK model compared to EML4-ALK. *Cancer Med.* **2015**, *4*, 953–965.

- (35) Ardini, E.; Menichincheri, M.; Banfi, P.; Bosotti, R.; De Ponti, C.; Pulci, R.; Ballinari, D.; Ciomei, M.; Texido, G.; Degrassi, A.; Avanzi, N.; Amboldi, N.; Saccardo, M. B.; Casero, D.; Orsini, P.; Bandiera, T.; Mologni, L.; Anderson, D.; Wei, G.; Harris, J.; Vernier, J.-M.; Li, G.; Felder, E.; Donati, D.; Isacchi, A.; Pesenti, E.; Magnaghi, P.; Galvani, A. Entrectinib, a pan-TRK, ROS1, and ALK inhibitor with activity in multiple molecularly defined cancer indications. *Mol. Cancer Ther.* **2016**, DOI: 10.1158/1535-7163.MCT-15-0758.
- (36) Colombo, M.; Sirtori, F. R.; Rizzo, V. A fully automated method for accurate mass determination using high-performance liquid chromatography with a quadrupole/orthogonal acceleration time-of-flight mass spectrometer. *Rapid Commun. Mass Spectrom.* **2004**, *18*, 511–517.
- (37) Felder, E. R.; Badari, A.; Disingrini, T.; Mantegani, S.; Orrenius, C.; Avanzi, N.; Isacchi, A.; Salom, B. The generation of purinome-targeted libraries as a means to diversify ATP-mimetic chemical classes for lead finding. *Mol. Diversity* **2012**, *16*, 27–51.
- (38) Winn, M. D.; Ballard, C. C.; Cowtan, K. D.; Dodson, E. J.; Emsley, P.; Evans, P. R.; Keegan, R. M.; Krissinel, E. B.; Leslie, A. G. W.; McCoy, A.; McNicholas, S. J.; Murshudov, G. N.; Pannu, N. S.; Potterton, E. A.; Powell, H. R.; Read, R. J.; Vagin, A.; Wilson, K. S. Overview of the CCP4 suite and current developments. *Acta Crystallogr., Sect. D: Biol. Crystallogr.* **2011**, *D67*, 235–242.
- (39) McCoy, A. J.; Grosse-Kunstleve, R. W.; Adams, P. D.; Winn, M. D.; Storoni, L. C.; Read, R. J. Phaser crystallographic software. *J. Appl. Crystallogr.* **2007**, *40*, 658–674.
- (40) Emsley, P.; Cowtan, K. (2004) Coot: Model-building tools for molecular graphics. *Acta Crystallogr., Sect. D: Biol. Crystallogr.* **2004**, *D60*, 2126–2132.
- (41) Murshudov, G. N.; Vagin, A. A.; Dodson, E. J. Refinement of Macromolecular Structures by the Maximum-Likelihood method. *Acta Crystallogr., Sect. D: Biol. Crystallogr.* **1997**, *D53*, 240–255.
- (42) Delano, W. L. *The PyMol Molecular Graphics System*; DeLano Scientific LLC, Palo Alto, CA, 2008.
- (43) Pevalotto, P.; Brasca, M. G.; Amici, R.; Orsini, P.; Traquandi, G.; Corti, L.; Piutti, C.; Sansonna, P.; Villa, M.; Pierce, B. S.; Pulici, M.; Giordano, P.; Martina, K.; Fritzen, E. L.; Nugent, R. A.; Casale, E.; Cameron, A.; Ciomei, M.; Roletto, F.; Isacchi, A.; Fogliatto, G.; Pesenti, E.; Pastori, W.; Marsiglio, A.; Leach, K. L.; Clare, P. M.; Fiorentini, F.; Varasi, M.; Vulpetti, A.; Warpehoski, M. A. 3-Aminopyrazole inhibitors of CDK2/Cyclin A as antitumor agents. 1. Lead finding. *J. Med. Chem.* **2004**, *47*, 3367–3380.
- (44) Kerns, E. H.; Di, L.; Petusky, S.; Farris, M.; Ley, R.; Jupp, P. Combined application of parallel artificial membrane permeability assay and Caco-2 permeability assays in drug discovery. *J. Pharm. Sci.* **2004**, *93*, 1440–1453.
- (45) Beria, I.; Ballinari, D.; Bertrand, J. A.; Borghi, D.; Bossi, R. T.; Brasca, M. G.; Cappella, P.; Caruso, M.; Ceccarelli, W.; Ciavolella, A.; Cristiani, C.; Croci, V.; De Ponti, A.; Fachin, G.; Ferguson, R. D.; Lansen, J.; Moll, J. K.; Pesenti, E.; Posteri, H.; Perego, R.; Rocchetti, M.; Storici, P.; Volpi, D.; Valsasina, B. Identification of 4,5-Dihydro-1H-pyrazolo[4,3-h]quinazoline Derivatives as a New Class of Orally and Selective Polo-Like Kinase 1 Inhibitors. *J. Med. Chem.* **2010**, *53*, 3532–3551.
- (46) Bao, R.; Lai, C. J.; Qu, H.; Wang, D.; Yin, L.; Zifcak, B.; Atoyan, R.; Wang, J.; Samson, M.; Forrester, J.; DellaRocca, S.; Xu, G. X.; Tao, X.; Zhai, H. X.; Cai, X.; Qian, C. CUDC-305, a novel synthetic HSP90 inhibitor with unique pharmacologic properties for cancer therapy. *Clin. Cancer Res.* **2009**, *15*, 4046–4057.